Spin-orbit coupling induced orbital entanglement in a three-band Hubbard model

Petr A. Igoshev [1], Danil E. Chizhov [2], Valentin Yu. Irkhin [1], and Sergey V. Streltsov [1,2]

[1]*Institute of Metal Physics, S. Kovalevskaya Street 18, 620108 Ekaterinburg, Russia*

[2]*Department of Theoretical Physics and Applied Mathematics, Ural Federal University, Mira Street 19, 620002 Ekaterinburg, Russia*

The effect of the spin-orbit coupling on the ground state properties of the square-lattice three-band Hubbard model with a single electron per site is studied by a generalized Hartree-Fock approximation. We calculate the full phase diagram and show that there appear additional orbital-entangled phases brought about by competition of various exchange channels or by the spin-orbit coupling in addition to conventional states stabilized by the Kugel-Khomskii mechanism. One of these phases previously proposed to explain magnetic properties of Sr_2VO_4 is characterized by vanishing dipolar magnetic moments and antiferro-octupolar ordering. We calculated microscopic parameters for this material and demonstrate that it is located near a phase boundary of two orbital-entangled and two conventional antiferromagnetic ferro-orbital states.

I. INTRODUCTION

The Hubbard Hamiltonian on a square lattice has become not only one of the most studied models over the past decades, but has turned out to be a standard test bed for various theoretical methods. Nevertheless, this model still harbors intriguing physics to be uncovered. Two ingredients—orbital degeneracy and the spin-orbit coupling—substantially enrich the variety of physical phenomena described by this model.

Being a very important theoretical concept, the model is extremely useful for practical applications, and not only in connection with high-temperature superconductivity of cuprates, but for many other materials and phenomena including the Kugel-Khomskii mechanism of orbital ordering in K_2CuF_4 [1,2], unconventional superconductivity in Sr_2RuO_4 [3], orbital-selective physics in Ca_2RuO_4 [4], and the spin-orbit assisted Mott transition in Sr_2IrO_4 [5]. There are also other layered perovskites with transition metals forming a square lattice, which demonstrate intriguing and yet to be understood physical properties. Examples include the anomalous staircase field dependence of magnetization [6] together with half metallicity [7–9] and obscure spin state of Co (electronic configuration $3d^5$) in Sr_2CoO_4 [8–12], or Sr_2CrO_4 ($3d^2$) with a reversed crystal field [13], strong interplay between spin and orbital degrees of freedom [14], and possible formation of orbitally ordered states switchable by ultrafast optical spectroscopy [15] and destroyable by pressure [16].

Another example is Sr_2VO_4 with V^{4+} ions having ionic configuration $3d^1$. One might expect formation of a long-range magnetic order at low enough temperature and, indeed, there is an anomaly in magnetic susceptibility at ~ 100 K, but neutron measurements do not detect any magnetic moment even at 5 K [17]. μSR experiments evidence formation of an antiferromagnetic order below 8 K [18]. Various theoretical models have been proposed to resolve the problem of vanishing local magnetic moment in this material. In particular, Imai *et al.* found a complicated spin-orbital order and severe competition between various magnetic/orbital configurations

[19]. Jackeli and Khaliullin put forward an idea of a hidden magnetic order, when orbital and spin moments are reduced to zero at each lattice site, and magnetic octupole order instead [20]. The Jackeli-Khaliullin state is characterized by vanishing dipolar magnetic moment and antiferro-octupolar order with *two* nonzero octupolar moments transformed by two nonequivalent representations. Eremin *et al.* suggested an alternative state with nonvanishing but compensating each other orbital and spin moments [21]. Density functional theory calculations by Kim *et al.* stress the importance of frustration effects and argue that spin-liquid or spin-glass states can be realized at very low temperatures [22].

In the present paper we perform a detailed study of a three-orbital Hubbard model on the square lattice with a checkerboard order taking into account the spin-orbit coupling and tetragonal crystal-field splitting using a generalized Hartree-Fock approximation (HFA). Particular attention is paid to the situation of a single d electron, being characteristic for Sr_2VO_4. The ground state phase diagram and physical properties of each phase are discussed in detail. We show that Sr_2VO_4 is in a region of the phase diagram where two highly unusual states with orbital-entangled wave functions (one of which is characterized by zero dipolar but finite octupolar magnetic moment) and two more conventional states with ferromagnetic (but different antiferro-orbitally ordered configurations) are realized.

II. MODEL AND METHOD

The Hamiltonian of our model reads

$$\mathcal{H} = \mathcal{H}_t + \mathcal{H}_{CF} + \mathcal{H}_{so} + \mathcal{H}_{Coulomb}, \quad (1)$$

where the first term describes intersite hopping processes

$$\mathcal{H}_t = \sum_{ijmm'\sigma} t_{ij}^{mm'} c_{im\sigma}^\dagger c_{jm'\sigma}, \quad (2)$$

where $m, m' = xz, xy, yz$ numerate orbitals, $\sigma, \sigma' = \uparrow, \downarrow$ define spin projection, and $t_{ij}^{mm'}$ are hopping amplitudes between

corresponding orbitals on sites i and j. The second term

$$\mathcal{H}_{\mathrm{CF}} = \Delta_{\mathrm{CF}} \sum_{i\sigma} c^\dagger_{i,xy,\sigma} c_{i,xy,\sigma} \tag{3}$$

sets up tetragonal crystal-field splitting Δ_{CF}. The third term in Eq. (1) describes the spin-orbit coupling with the strength defined by the corresponding parameter λ,

$$\mathcal{H}_{\mathrm{so}} = -\lambda \sum_{i,mm'} \boldsymbol{\mathcal{S}}_{i;mm'} \cdot \boldsymbol{l}_{mm'}. \tag{4}$$

Here three components $o = 1, 2, 3$ of

$$\mathcal{S}^{(o)}_{i;mm'} = \frac{1}{2} \sum_{\sigma\sigma'} c^\dagger_{im\sigma} \sigma^o_{\sigma\sigma'} c_{im'\sigma'} \tag{5}$$

give (generalized) spin operators, and $o = 0$ provides information about interorbital occupation, σ^o are Pauli matrices, and $\mathbf{l}_{mm'}$ are conventional matrices of orbital momentum in the basis of cubic harmonics

$$l^x_{mm'} = \begin{pmatrix} 0 & -\mathrm{i} & 0 \\ +\mathrm{i} & 0 & 0 \\ 0 & 0 & 0 \end{pmatrix}, \quad l^y_{mm'} = \begin{pmatrix} 0 & 0 & 0 \\ 0 & 0 & -\mathrm{i} \\ 0 & +\mathrm{i} & 0 \end{pmatrix}, \tag{6}$$

$$l^z_{mm'} = \begin{pmatrix} 0 & 0 & +\mathrm{i} \\ 0 & 0 & 0 \\ -\mathrm{i} & 0 & 0 \end{pmatrix}. \tag{7}$$

The minus sign in Eq. (4) is needed to work with the t_{2g} orbitals, which can be modeled as effective p orbitals ($l = 1$), but with opposite sign of the spin-orbit coupling constant; see, e.g., [23,24].

The on-site Coulomb interaction is taken in the following form:

$$\begin{aligned}
\mathcal{H}_{\mathrm{Coulomb}} = {}& \frac{U}{2} \sum_{im\sigma} n_{im\sigma} n_{im\bar{\sigma}} + \frac{U'}{2} \sum_{i,m\neq m'} n_{im} n_{im'} \\
& - \frac{J_{\mathrm{H}}}{2} \sum_{im\neq m';\sigma\sigma'} c^\dagger_{i,m\sigma} c_{i,m\sigma'} c^\dagger_{i,m'\sigma'} c_{i,m'\sigma} \\
& - \frac{J_{\mathrm{d}}}{2} \sum_{im\neq m';\sigma} c^\dagger_{i,m\sigma} c_{i,m'\bar{\sigma}} c^\dagger_{i,m\bar{\sigma}} c_{i,m'\sigma},
\end{aligned} \tag{8}$$

where U (U') is the on-site Coulomb intraorbital (interorbital) interaction parameter, J_{H} is the Hund's intra-atomic exchange (in the Kanamori representation [25] $U = U' + 2J_{\mathrm{H}}$), pair-hopping matrix element $J_{\mathrm{d}} = J_{\mathrm{H}}$ is a real number, since we work with real cubic (t_{2g}) orbitals, and $n_{im\sigma} = c^\dagger_{im\sigma} c_{im\sigma}$ and $n_{im} = \sum_\sigma n_{im\sigma}$ are the occupation number operators. The notation $\bar{\sigma} = -\sigma$ is used.

Below we consider the case of a single electron per lattice site under the assumption that a two-sublattice checkerboard long-range order is established. In the case of a Mott-Hubbard insulator with an integer band filling the Hartree-Fock approximation provides reasonable results [26]. Indeed, in this case HFA yields correct energy values in the atomic limit, provided that virtual states are treated correctly within this method (i.e., essentially Anderson's kinetic exchange effects). This approximation was also successfully applied to describe the electron and magnon spectrum [26] and magnetic phase diagram of the two-band s-d exchange model [27].

Otherwise, HFA gives only a qualitative estimate of ground state energy missing a vertex correction to virtual state energies. However, the quality of HFA indeed depends on the phases considered and an estimation of its applicability is not straightforward.

Due to the local character of the Coulomb interaction Hamiltonian (8), the generalized HFA is fully specified by a *local order* characterized by a correlator

$$C^i_{m\sigma;m'\sigma'} \equiv \langle c^\dagger_{im\sigma} c_{im'\sigma'} \rangle. \tag{9}$$

See details of the derivation in Appendix B; see Eq. (B8).

We consider the decomposition of the correlator into a complete set of Pauli matrices

$$C^i_{m\sigma;m'\sigma'} = \mathfrak{n}^i_{mm'} \sigma^0_{\sigma'\sigma} + \mathfrak{m}^i_{mm'} \cdot \boldsymbol{\sigma}_{\sigma'\sigma}, \tag{10}$$

where

$$\mathfrak{n}^i_{mm'} = \langle \mathcal{S}^{(0)}_{i;mm'} \rangle, \tag{11}$$

$$\mathfrak{m}^i_{mm'} = \langle \boldsymbol{\mathcal{S}}_{i;mm'} \rangle \tag{12}$$

are the components of 4-component (charge-spin) vector $N^i_{mm'}(\mathfrak{n}^i_{mm'}, \mathfrak{m}^i_{mm'})$.

Fourier transform of an arbitrary field φ^i can be defined in a standard way $\varphi(\mathbf{q}) = (1/N) \sum_i \exp(i\mathbf{q}\mathbf{R}_i)\varphi^i$, where N is a number of lattice sites and $\mathbf{q}$ is a wave vector. For two-sublattice valued φ^i one can once again single out two components of a field φ

$$\varphi(\mathbf{q}) = \delta_{\mathbf{q}0}\varphi^{\mathrm{u}} + \delta_{\mathbf{q}\mathbf{Q}}\varphi^{\mathrm{s}}, \tag{13}$$

where φ^{u} (φ^{s}) is the uniform (staggered) component. We restrict ourselves to considering a two-sublattice ordering and take $\varphi^i = C^i_{m\sigma;m'\sigma'}$ with two components, a uniform (C^{u}) and staggered (C^{s}):

$$C^i_{m\sigma;m'\sigma'} = C^{\mathrm{u}}_{m\sigma;m'\sigma'} + \exp[i\mathbf{Q}\mathbf{R}_i] C^{\mathrm{s}}_{m\sigma;m'\sigma'} \tag{14}$$

(from a mathematical point of view, this limits a class of the general HFA equation solutions). This approach provides all two-sublattice long-range order solutions for within HFA. Thereby, we take into account that the ordering has only two components (uniform and staggered), see Eqs. (13) and (14), so that the Fourier transforms of $\mathfrak{n}^i_{mm'}$ and $\mathfrak{m}^i_{mm'}$ have only $\mathbf{q} = \mathbf{0}$, $\mathbf{Q}$ nonzero contributions (see Appendix B).

Within the Hartree-Fock approximation, the total Hamiltonian reads

$$\begin{aligned}
\mathcal{H}_{\mathrm{MF}} = {}& \sum_{\mathbf{k}_1\mathbf{k}'_1;mm'} \sum_{\sigma\sigma'} \big([\varepsilon_{mm'}(\mathbf{k}_1)\delta_{\sigma\sigma'} + \mathcal{F}^{(0)\mathrm{u}}_{mm'}\delta_{\sigma\sigma'} \\
& - \mathcal{F}^{\mathrm{u}}_{mm'}\boldsymbol{\sigma}_{\sigma\sigma'} - (\lambda/2)\mathbf{l}_{mm'}\boldsymbol{\sigma}_{\sigma\sigma'}]\delta_{\mathbf{k}_1\mathbf{k}'_1} \\
& + [\mathcal{F}^{(0)\mathrm{s}}_{mm'}\delta_{\sigma\sigma'} - \boldsymbol{\mathcal{F}}^{\mathrm{s}}_{mm'} \cdot \boldsymbol{\sigma}_{\sigma\sigma'}]\delta_{\mathbf{k}_1,\mathbf{k}'_1+\mathbf{Q}}\big) c^\dagger_{\mathbf{k}_1 m\sigma} c_{\mathbf{k}'_1 m'\sigma'},
\end{aligned} \tag{15}$$

where mean fields $\mathcal{F}^{(0)i}_{mm'}$ and $\boldsymbol{\mathcal{F}}^i_{mm'}$ generally have complex orbital structure

$$\begin{aligned}
\mathcal{F}^{(0)i}_{mm'} = {}& -(U' - 2J_{\mathrm{H}})\mathfrak{n}^i_{m'm} + J_{\mathrm{d}}\mathfrak{n}^i_{mm'} \\
& + \delta_{mm'}(2U' - J_{\mathrm{H}}) \sum_{m''} \mathfrak{n}^i_{m''m''},
\end{aligned} \tag{16}$$

$$\boldsymbol{\mathcal{F}}^i_{mm'} = U'\mathfrak{m}^i_{m'm} + J_{\mathrm{d}}\mathfrak{m}^i_{mm'} + \delta_{mm'}J_{\mathrm{H}} \sum_{m''} \mathfrak{m}^i_{m''m''}, \tag{17}$$

and analogous expressions hold for uniform and staggered components of $\mathcal{F}^{(0)}$ and $\mathcal{F}$: this corresponds to the replacement $i \rightarrow$ u and s in Eqs. (16) and (17) correspondingly. The detailed derivation of Eqs. (16) and (17) is given in Appendix B.

From Eqs. (5), (11)–(14), see also Eq. (B28) in Appendix B, we get the system of mean-field equations in terms of 4-vectors $N_{mm'}^{\mathrm{u}}(\mathfrak{n}_{mm'}^{\mathrm{u}}, \mathfrak{m}_{mm'}^{\mathrm{u}})$ and $N_{mm'}^{\mathrm{s}}(\mathfrak{n}_{mm'}^{\mathrm{s}}, \mathfrak{m}_{mm'}^{\mathrm{s}})$

$$N_{mm'}^{(o)\mathrm{u}} = \frac{1}{2N} \sum_{\mathbf{k}\alpha\sigma}' \sigma_{\sigma\sigma'}^{o} F_{m\alpha\sigma;m'\alpha\sigma'}(\mathbf{k}), \tag{18}$$

$$N_{mm'}^{(o)\mathrm{s}} = \frac{1}{2N} \sum_{\mathbf{k}\alpha\sigma}' \sigma_{\sigma\sigma'}^{o} F_{m\alpha\sigma;m'\bar{\alpha}\sigma'}(\mathbf{k}), \tag{19}$$

where $o = 0, 1, 2, 3$; a prime over sums denotes summation over the magnetic Brillouin zone and

$$F_{m\alpha\sigma;m'\alpha'\sigma'}(\mathbf{k}) = \sum_{\nu} a_{m\alpha\sigma;\nu}^{*}(\mathbf{k}) a_{m'\alpha'\sigma';\nu}(\mathbf{k}) f(E_{\nu}(\mathbf{k})), \tag{20}$$

where $a_{m\alpha\sigma;\nu}$ are eigenvectors belonging to eigenvalue E_{ν} of the matrix of the single-electron version of Hamiltonian (15), see Eq. (B25) in Appendix B, $f(E) = \{\exp[(E - E_{\mathrm{F}})/T] + 1\}^{-1}$ is the Fermi function, and E_{F} is the Fermi level. Within our HFA approach, the latter is adjusted to set the filling equal to one electron per site.

We get the expression for the full energy within HFA, $\mathcal{E} = \langle \mathcal{H}_{\mathrm{MF}} \rangle$,

$$\mathcal{E}/N = \frac{1}{N} \sum_{\mathbf{k}\nu} E_{\nu}(\mathbf{k}) f(E_{\nu}(\mathbf{k})) - E_{\mathrm{DC}}/N, \tag{21}$$

where residual terms of HFA are absorbed into E_{DC}; see Eq. (B29) in Appendix B.

The above-presented formalism can be applied in the case of an arbitrary filling, not only 1/6 occupation (one electron per site). The filling is controlled only by E_{F}. However, the quality of an approximation depends dramatically on whether integer or noninteger filling per site situation is considered. In the latter case, for large U, strong electron correlations renormalize the electron spectrum, so that more elaborated approximations like dynamical mean-field theory (DMFT) or the Kotliar-Ruckenstein slave-boson approximation [28] (see also calculations in Refs. [29,30]) should be employed. In the case of integer filling, HFA is a reasonable approximation.

Finally, we turn to choice of specific parameters. There is an intrinsic deformation—elongation of transition metal octahedra in layered perovskites, which are physical realizations of a square lattice. This results in such a splitting of the t_{2g} shell that the xy orbital goes higher in energy (by Δ_{CF}) than the xz/yz doublet; see Fig. 1(a). Another structural feature characteristic for this class of materials is symmetry of hopping parameters. There is always hopping between the xy orbitals on nearest-neighbor sites $t_{xy/xy} = t$, but the yz orbitals overlap (directly or via the p_z orbital of a ligand) with its partner only along one of the directions (a bond in Fig. 2), so that $t_{yz/yz}^{a} = t$ and $t_{xz/xz}^{a} = 0$. The electrons on the last orbital, xz, can also hop only along half of metal–metal bonds (b bond in Fig. 2): $t_{xz/xz}^{b} = t$ and $t_{yz/yz}^{b} = 0$. Thus, the explicit expressions
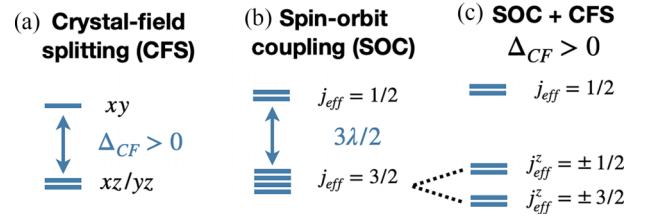

FIG. 1. Illustration of effects of (a) the crystal-field splitting given by (3) (positive Δ_{CF} corresponds to elongation of octahedra surrounding transition metals), (b) the spin-orbit coupling (4), and (c) their combined action in the case of $\lambda > \Delta_{\mathrm{CF}} > 0$, which shifts states of $|j_{\mathrm{eff}} = 3/2, j_{\mathrm{eff}}^{z} = \pm 1/2\rangle$ up in energy.

for the band dispersion reads as $\varepsilon_{xy,xy}(\mathbf{k}) = -2t(\cos k_x + \cos k_y)$, $\varepsilon_{xz,xz}(\mathbf{k}) = -2t \cos k_x$, $\varepsilon_{yz,yz}(\mathbf{k}) = -2t \cos k_y$.

Next-nearest-neighbor hopping t' can result in breaking the nesting condition and prevent a metal-insulator transition [31,32], provided that $(U - 3J_{\mathrm{H}})/t$ is sufficiently small. But this case is beyond our consideration.

III. POSSIBLE STATES AND PHASE DIAGRAM: NO SPIN-ORBIT COUPLING

We start from a somewhat simplified consideration assuming that electrons are localized on particular cubic harmonics, and then go on taking into account quantum effects which result in more complex states obtained by the Hartree-Fock method.

Conventional ferro- and antiferro-orbital states. Without the spin-orbit coupling and for a large and positive crystal-field splitting (i.e., with elongated metal-ligand octahedra), one might expect that in the ground state sites the half-filled xz and yz orbitals will alternate. There is a hopping between half-filled and empty orbitals [antiferro-orbital (AFO) order] for all bonds in this state. This hopping favors ferromagnetic coupling according to Goodenough-Kanamori-Anderson (GKA) rules [33–35]. Such a state is shown in Fig. 3(a) and Fig. 4(a) and referred to as FM-AFO$_{xz/yz}$ in what follows. This type of orbital and magnetic order is favored by Hund's intra-atomic
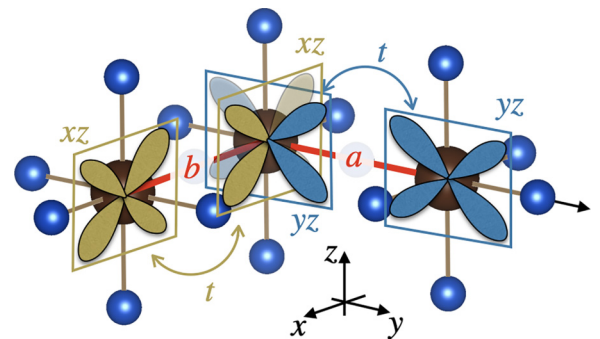

FIG. 2. Sketch illustrating overlap of xz/yz orbitals in the crystal structure of layered perovskites. Transition metals are shown by brown balls, while ligands are blue. There is an overlap between the yz orbitals in one of the directions (a). This orbital stays silent in another direction (b), while the xz orbitals strongly overlap. There is also overlap between the xy orbitals in both directions (not shown).
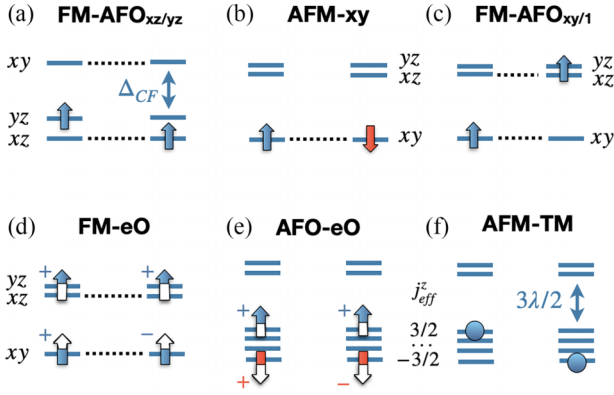
FIG. 3. Sketch illustrating various states for a pair of neighboring sites; corresponding charge-density plots are presented in Fig. 4. Possible hopping paths for (a)–(d) are shown by dashed lines. In the FM-AFO$_{xz/yz}$ (ferromagnetic–antiferro-orbital) configuration, one electron is at the yz orbital, while another one resides at xz, and hopping from site to site favors FM spin ordering. Very similar is the situation for FM-AFO$_{xy/1}$ (xy on one site and $|l_{eff}^z| = 1$ on another are occupied). In the AFM-xy state hopping between the xy orbitals stabilizes AFM order. The other two states, FM-eO and AFO-eO, are orbital-entangled states. The exact wave functions for them are given in (23) and (24). We sketched these wave functions via noncomplete filling of arrows denoting spins; plus and minus signs are used to show the phase of wave functions. In the last AFM-TM state electrons occupy $j_{eff}^z = 3/2$ or $j_{eff}^z = -3/2$ depending on the sublattice (TM stands for the total moment).

exchange J_H and large crystal-field field Δ_{CF} [35] and realized, e.g., in perovskite YTiO$_3$ [36].

An alternative AFM-xy state is shown in Fig. 3(b) and Fig. 4(b). Electrons occupy the xy orbital at all sites in this case. This ferro-orbital (FO) ordering is stabilized by a small positive or negative Δ_{CF} and, according to GKA rules, leads to the antiferromagnetic (AFM) state.
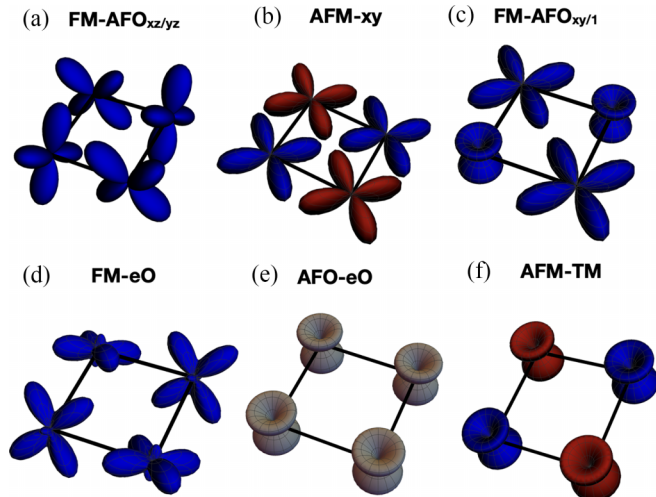

FIG. 4. Charge densities for various electronic states under consideration; see Fig. 3. Two different spins are shown by blue and red. Gray color is used for AFO-eO, where the spin moment vanishes.
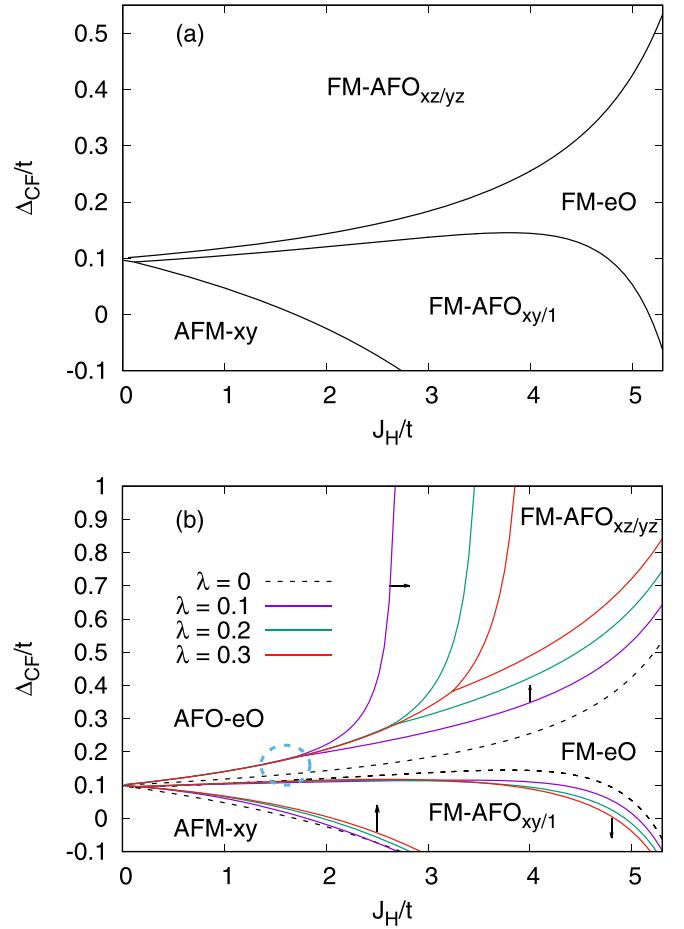

FIG. 5. Ground state phase diagram for the crystal-field splitting $-0.1t < \Delta_{CF} < 1.0t$ without (a) and taking into account (b) the spin-orbit coupling. Here J_H stands for the Hund's intra-atomic exchange, λ is the spin-orbit coupling constant, t is the hopping, and Hubbard's parameter is $U = 20t$. Sketches of different states are shown in Figs. 3 and 4. An increase of λ results in an expansion of AFO-eO phase region to the right, an expansion of FM-eO phase region upward, and contraction of FM-AFO$_{xz/yz}$ (the directions of phase boundaries moving are shown by arrows). In (b) black dotted line shows the result for $\lambda = 0$ [the same as in Fig. 5(a)] for the sake of convenience. Blue circle indicates the region of relevance for Sr$_2$VO$_4$ parameters (close to $J_H = 1.6t$, $\Delta_{CF} = 0.16t$); see Sec. VI.

The full phase diagram including these two states obtained by the Hartree-Fock method is presented in Fig. 5(a). It was calculated by direct solution of the nonlinear self-consistent system (independent 71 variables) of Eqs. (18) and (19) comparing full energies of different phases in the $T \to 0$ limit; see Eqs. (21) and (B29). The self-consistency process starts with choice of initial states and iterative procedure modifying them. Brillouin zone integration in **k** space was performed by triangular method [37] for $N_{grid} = 40$ triangles.

Negative crystal-field splitting Δ_{CF} (when the xy orbital gets lower than the xz/yz doublet) obviously stabilizes the AFM-xy state, but it is realized even for small and positive Δ_{CF}. This is because for AFM-xy both electrons tunnel and lower the total energy for any bond, while for FM-AFO$_{xz/yz}$ only one electron can hop along each bond (yz for bond a and

xz for bond *b*). On the other hand, one can see from Fig. 5 that the AFM-*xy* state is destabilized by the Hund's coupling. In this case the energy of the excited state E_{exc} (due the hopping) is strongly reduced by J_H in the case of FM-AFO$_{xz/yz}$ (one electron is on *xz*, while another one is on the *yz* orbital; $E_{\text{exc}} = U - 3J_H$, if we use the Kanamori parametrization [25]) with respect to what we have for AFM-*xy* (both electrons are on the *xy* orbital; $E_{\text{exc}} = U$).

However, strong Hund's coupling stabilizes not FM-AFO$_{xz/yz}$, but a very different state, with electrons occupying the *xy* orbital on sublattice A and an arbitrary superposition of the *xz* and *yz* orbitals with the same spin projection on the B sublattice. For example, one can chose the following wave function,

$$\big| l_{\text{eff}}^z = 1 \big\rangle = -\frac{1}{\sqrt{2}}(|yz\rangle + \mathrm{i}|xz\rangle); \tag{22}$$

see in Fig. 3(c) and Fig. 4(c). We note that any other mixture of the *xz* and *yz* orbitals can be used without the spin-orbit coupling. In this FM-AFO$_{xy/1}$ state we win both by intra-atomic exchange (in the excited state both electrons have the same spin) and by a very efficient hopping of electrons on the *xy* orbitals. This state is doubly degenerate with respect to spin [if we take into account the spin-orbit coupling the spin-down electrons occupy the $|l_{\text{eff}}^z = -1\rangle = (|yz\rangle - \mathrm{i}|xz\rangle)/\sqrt{2}$ orbital on sublattice B].

FM-eO phase with entangled orbitals (eO). However, hopping can be optimized even further on mixing *xy* and *yz/xz* orbitals (or their linear combinations given by $l_{\text{eff}}^z = \pm 1$) in an appropriate way. This new phase is characterized by FM coupling and referred to as FM-eO. In the case of degenerate t_{2g} orbitals ($\Delta_{\text{CF}} = 0$) one can find the wave functions for two sites forming a checkerboard order analytically [38]:

$$A : \frac{2}{3}|xy, \sigma\rangle + \frac{\sqrt{5}}{3}| l_{\text{eff}}^z = 1, \sigma\rangle,$$
$$B : \frac{2}{3}|xy, \sigma\rangle - \frac{\sqrt{5}}{3}| l_{\text{eff}}^z = 1, \sigma\rangle, \tag{23}$$

where A and B are two sublattices, and σ stands for spin. It has to be mentioned that this solution is degenerate with respect to $\sigma \to -\sigma$ and $l_{\text{eff}}^z \to -l_{\text{eff}}^z$ inversions separately. However, for a finite spin-orbit coupling, see below, only the symmetry $(l_{\text{eff}}^z, \sigma) \to (-l_{\text{eff}}^z, -\sigma)$ remains. Second, it is remarkable that two sublattices differ only by the phase of $| l_{\text{eff}}^z = 1, \sigma\rangle$ component. Finally, in a general case of arbitrary Δ_{CF} exact expression for wave functions depends on parameters and changes in different points of the phase diagram. This is in contrast to the AFO-eO phase discussed in Sec. IV.

At $J_H = 0$ only AFM-*xy* and FM-AFO$_{xz/yz}$ are presented: the critical point is determined by competition of (intersite) exchange $J_{\text{ex}} = t^2/U$ and the crystal-field splitting Δ_{CF}: $\Delta_{\text{CF}}^* = 2J_{\text{ex}}$. Stability of the FM-eO and FM-AFO$_{xy/1}$ phases is rapidly increased and corresponding regions on the phase diagram expand as J_H increases. Parameters corresponding to Sr_2VO_4 at normal conditions are presented Sec. VI. They are rather close to the phase boundary between the FM-AFO$_{xz/yz}$, FM-AFO$_{xy/1}$, and FM-eO states, but the phase diagram by itself strongly changes by the spin-orbit coupling as we show in the next section.

IV. PHASE DIAGRAM AT FINITE SPIN-ORBIT COUPLING

AFO-eO phase stabilized by SOC. Generally speaking, the crystal-field splitting and the spin-orbit coupling (SOC) tend to stabilize electrons on quite different orbitals. The first one prefers real (cubic) wave functions, while the second prefers complex spherical harmonics (this can be critical, in particular, for the Jahn-Teller effect [39,40]). The intra-atomic exchange J_H favors a maximal total spin (in our situation this is important for virtual excited states with two electrons per site), whereas wave functions stabilized by SOC can mix different spin components; see, e.g., Eqs. (28) and (29) in Ref. [35]. Therefore, SOC must affect the phase diagram of the three-orbital Hubbard model described above.

First of all, SOC is expected to influence the states with partially filled degenerate *xz/yz* orbitals, i.e. the situation shown in Fig. 1(a) corresponding $\Delta_{\text{CF}} > 0$. Indeed, one can always gain some energy due to the SOC putting our electron on a linear combination of these orbitals corresponding to $l_{\text{eff}}^z = 1$; see Eq. (22). This is shown in Fig. 1(c), where the $j_{\text{eff}} = 3/2$ quartet is split by a positive crystal field on two Kramers doublets: $j_{\text{eff}}^z = \pm 1/2$ and $j_{\text{eff}}^z = \pm 3/2$. The results of direct Hartree-Fock calculations presented in Fig. 5(b) demonstrate that even a modest SOC with $\lambda = 0.1t$ leads to shift of the FM-AFO$_{xz/yz}$ state to the region of large J_H and to formation of a novel AFO-eO phase, sketched in Fig. 3(e) and Fig. 4(e). The wave function in this new phase is written in a very simple form:

$$\frac{1}{\sqrt{2}}\big(\big| l_{\text{eff}}^z = 1, \uparrow \big\rangle \pm \big| l_{\text{eff}}^z = -1, \downarrow \big\rangle \big), \tag{24}$$

where different signs are taken for two different sublattices (A or B). This AFO-eO state is exactly the state with staggered order of in-plane confined isospins, found by Jackelli and Khaliullin in [20]. Dipole spin

$$\mathbf{S}_i = \sum_m \boldsymbol{\mathcal{S}}_{imm} \tag{25}$$

[with generalized spin operator $\boldsymbol{\mathcal{S}}_{imm}$ defined in (5)] and orbital $\mathbf{L}_i$ moments vanish at every lattice site $\langle \mathbf{S}_i \rangle = \langle \mathbf{L}_i \rangle = 0$, so that only octupole moments remain nonzero and they order in a staggered fashion, as we will discuss below.

Higher-lying in energy AFM-TM *phase.* A very different state was considered in [21]. In particular, the electron can be localized not on a linear combination of $|j_{\text{eff}}^z = +3/2\rangle$ and $|j_{\text{eff}}^z = -3/2\rangle$ at the given sublattice as in the case of the AFO-eO state, but it can be described by "pure" $\psi_A = |j_{\text{eff}}^z = +3/2\rangle$ at the A and $\psi_B = |j_{\text{eff}}^z = -3/2\rangle$ at the B sublattice. The latter situation is shown in Figs. 3(f) and 4(f) and dubbed as AFM-TM (total angular momentum antiferromagnetism). Spin and orbital momenta exist on each site in this case, but cancel each other, as explained in [21].

We performed an accurate consideration of the energies of both AFO-eO and AFM-TM states within the mean-field approximation for the kinetic exchange Hamiltonian derived from Eq. (1) in the limit $zt \ll U - 3J_H$ using the formalism developed in [38] (z is the coordination number; see Appendix A for details). While both these states are stabilized mainly by spin-orbit coupling, in the leading (zeroth) order with respect to λ and Δ_{CF} the kinetic exchange Hamiltonian yields that the AFO-eO state has a lower energy than the
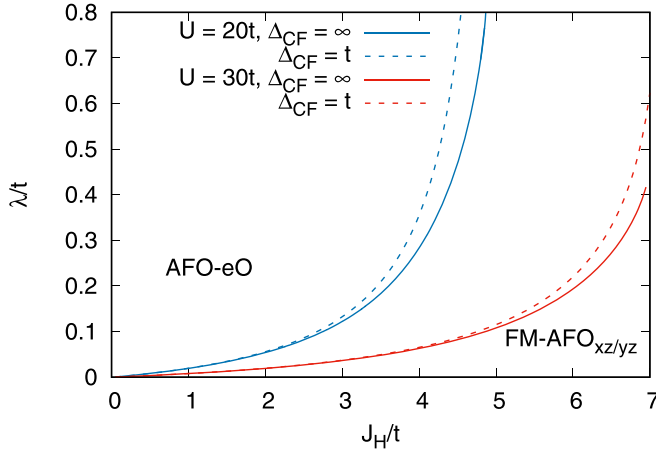
FIG. 6. Ground state phase diagram for large ($\Delta_{CF} = 1.0t$; dashed lines) or infinite ($\Delta_{CF} = \infty$; solid lines) in terms of J_H and λ. Blue (red) lines show the $U = 20t$ ($30t$) case. Two phases, FM-AFO$_{xz/yz}$ and AFO-eO, are considered.

AFM-TM state due to the explicitly nonsymmetric (with respect to $i \leftrightarrow j$) *ferromagnetic* exchange contribution in the effective Hamiltonian

$$\mathcal{H}_{non-symm} = -\frac{2J_H}{(U - 3J_H)(U - J_H)} \sum_{ijm} |t_{ij}^m|^2 \mathcal{S}_{imm} \mathbf{S}_j. \quad (26)$$

See the derivation in Appendix B. It can be readily shown that for the AFM-TM state this term is strictly positive whereas for the AFO-eO state it vanishes (all other terms in the kinetic exchange Hamiltonian yield the same result for both states). This analytic result can be compared with direct Hartree-Fock calculations presented in Fig. 8 in the Appendix A. Both approaches clearly show that AFM-TM is always higher in energy than AFM-TM and for small J_H this difference is well described by (26).

Competition of AFO-eO/FM-eO *and* FM-AFO$_{xz/yz}$ *phases.* Coming back to the AFO-eO phase one can notice that SOC is very efficient in suppression of the standard FM-AFO$_{xz/yz}$ state even at relatively large J_H; see Fig. 5(b). There is a very similar effect on narrowing the phase region of FM-AFO$_{xz/yz}$ state and expansion of not only the AFO-eO phase, but the FM-eO solution with increasing SOC as well.

For comparison, in Fig. 6 we present the phase diagram in other ($J_H - \lambda$) variables for a typically (realized experimentally) situation of positive and large Δ_{CF}. Such a crystal field shifts the xy orbital upward and this destabilizes the AFM-xy and FM-eO phases [where electrons occupy the xy orbital; see Figs. 3(b) and 3(d)], so that only the AFO-eO and FM-AFO$_{xz/yz}$ states survive. At small and moderate Hund's exchange, the AFO-eO solution dominates being stabilized by finite λ. In contrast, large J_H favors the FM-AFO$_{xz/yz}$ state. Indeed, excited (intermediate) states in the exchange processes for the FM-AFO$_{xz/yz}$ solution obey Hund's rule (these are triplet states like $xz_\uparrow yz_\uparrow$). Excited states for the AFO-eO phase do not completely optimize intra-atomic exchange interaction.

The lowering of Δ_{CF} favors the FM-AFO$_{xz/yz}$ phase which changes the phase diagram by expansion of the corresponding phase region quantitatively, but not qualitatively. However the

properties of the latter state strongly depend on parameter values, as explained in the next section. Last but not least, there is a strong influence of Hubbard U on the phase diagram, which is clearly seen in Fig. 6.

Order parameters. While the FM-AFO$_{xz/yz}$, FM-AFO$_{xy/1}$, AFM-TM, and FM-eO states can be characterized by standard order parameters—dipole moments $\langle \mathbf{L}_i \rangle$ and $\langle \mathbf{S}_j \rangle$ on corresponding sublattices $i = \{A, B\}$—in AFM-eO both such parameters vanish, as we have discussed above (hidden orbital-spin order [20]).

The AFM-eO state is stabilized by strong SOC putting electrons on the spin orbitals characterized by the total angular moment $\mathbf{J}$ (in our case $\mathbf{j}_{\text{eff}}$). It is instructive to consider expectation values of not only dipole (transforming according to Γ_4 representation of cubic group), but also quadrupole (Γ_3 and Γ_5 representations) and octupole (Γ_2, Γ_4, and Γ_5 representations) moments, which can be expressed via corresponding combinations of $\mathbf{J}$ components [41].

Our situation is characterized by the tetragonal symmetry in which Γ_4 and Γ_5 representations are reducible and direct calculations show that only two out of seven octupoles, $\langle T_x^\alpha \rangle$ and $\langle T_x^\beta \rangle$, transforming over corresponding one-dimensional irreducible representations, are nonzero for the AFM-eO state (all dipoles and quadrupoles vanish). There is antiferrooctupole ordering for both of them (nearest neighbors have opposite octupole moments). Moreover, on the same lattice site $\langle T_x^\alpha \rangle$ and $\langle T_x^\beta \rangle$ have the same sign.

V. MODIFICATION OF THE KUGEL-KHOMSKII FM-AFO$_{xz/yz}$ ORDER BY SOC

As shown in the previous section, while SOC generates new states having different anomalous properties such as vanishing dipole magnetic moment, it also modifies conventional states stabilized by the kinetic exchange. In this section we consider the evolution of the FM-AFO$_{xz/yz}$ state with increasing SOC.

In Fig. 7 we present decomposition of the occupied state (obtained by diagonalization of the on-site occupation matrix for one of sublattices) in cubic harmonics. In the case of very large crystal field, $\Delta_{CF} = \infty$, presented in the upper panel of Fig. 7, we have a conventional FM-AFO$_{xz/yz}$ with the electron sitting mostly at the $xz \uparrow$ orbital (for the second sublattice it will be $yz \uparrow$). The intra-atomic Hund's exchange works for this state due to the gradually reducing contribution of other orbitals caused by a finite SOC, $\lambda = 0.1t$.

However, a further increase of λ (up to $0.3t$) changes the situation dramatically. The SOC is nearly incapable of struggling with a too large crystal field and therefore faintly affects the xy orbital. In contrast, it mixes the xz and yz orbitals to form $l_{\text{eff}}^z = \pm 1$ states with the same spin projection, (22), which are eigenfunctions of SOC. This allows a gain in energy as much as possible, both in the crystal field and SOC contributions, but breaks the first Hund's rule. As a result, for fixed $\lambda > 0$ there exists a critical J_H^* below which occupations of $xz \uparrow$ and $yz \uparrow$ coincide [coefficients at corresponding wave functions are close to $1/\sqrt{2}$, see Fig. 7(a), while orbital occupancies equal 0.5]. The price to pay is a reduced energy gain due to kinetic exchange. For a finite crystal field, one observes a quite similar tendency of mixing the xz and yz
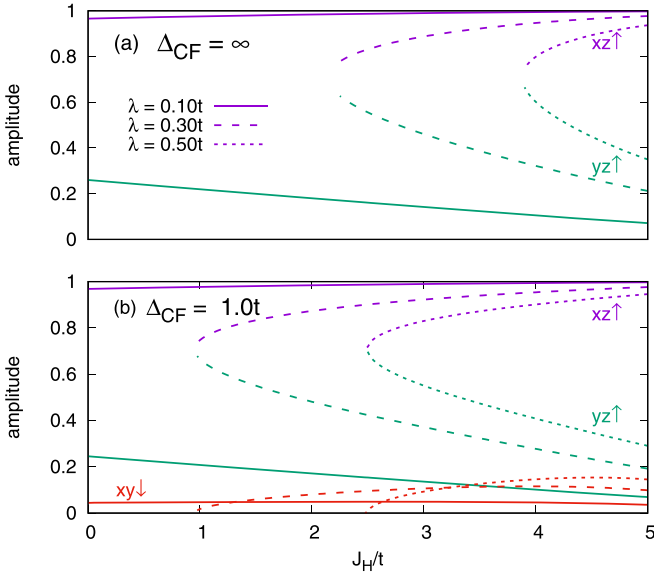
FIG. 7. Absolute value of wave function amplitudes of the FM-AFO$_{xz/yz}$ state for one of the sublattices depending on J_H at $\Delta_{CF} = \infty$ (a) and $\Delta_{CF} = 1.0t$ (b), where t is the hopping. Solid lines correspond to $\lambda = 0.1t$, dashed lines to $\lambda = 0.3t$, dotted lines to $\lambda = 0.5t$. Contribution of $xz \uparrow$ states is shown in violet, $yz \uparrow$ in green, and $xy \downarrow$ in red.

orbitals and onset of critical J_H^*; see Fig. 7(b). We also find that lowering Δ_{CF} stabilizes the FM-AFO$_{xz/yz}$ state, increasing the difference in occupation of the $xz \uparrow$ and $yz \uparrow$ orbitals as well as a nonvanishing contribution of the $xy \downarrow$ state.

VI. APPLICATION TO Sr$_2$VO$_4$

As explained in the introduction section, a physical realization of the three-orbital Hubbard model on a square lattice with a single electron is Sr$_2$VO$_4$ with quite unusual magnetic properties, which are still to be understood. We performed density function calculations of Sr$_2$VO$_4$ taking experimental crystal structure [17]. Further details are as follows: Approximation for the exchange-correlation potential was chosen following Perdew, Burke, and Ernzerhof (PBE) [42], the VASP code [43] was applied, and the projector augmented-wave method [44] together with integration over tetrahedra [45] with 405 **k** points was used; for projection onto a small Hamiltonian with only t_{2g} orbitals we applied the projected localized orbitals technique [46]. Some restricted set of orbital orders and collective excitations above them were considered within HFA to describe Sr$_2$VO$_4$ in the three-orbital Hubbard model at particular values of model parameters [47]. However, the complete ground state phase diagram and some important states were not considered there.

The hopping between the xz/yz orbitals was found to be $t = 250$ meV (very close to the previous estimate [48]), while the crystal-field splitting within t_{2g} is $\Delta_{CF} = 40$ meV (i.e., xy orbital lies higher than the xz/yz doublet), so that $\Delta_{CF}/t = 0.16$. The spin-orbit coupling constant for V^{3+} is about 30 meV ($\lambda/t = 0.12$) [23].

The constrained random-phase approximation (cRPA) has been used in Ref. [22] to calculate interaction parameters.

For the t_{2g}-only model used in the present work they turn out be $U = 2.7$ eV and $J_H = 0.4$ eV ($U = 11t$, $J_H = 1.6t$) [49]. In other papers, Hubbard's U varies from 3 to 5.3 eV ($U = 12 - 21t$) [22,50,51], depending on how exactly U is calculated and what is included in screening channels. One can see that with these characteristic parameters Sr$_2$VO$_4$ is situated very close to boundaries of the AFO-eO, FM-eO, FM-AFO$_{xz/yz}$, and FM-AFO$_{xy/1}$ phases; see Fig. 5(b). Thus suppressed magnetic moment (or its absence) can be related to formation of orbital entangled AFO-eO or FM-eO states, depending on the specific parameters realized in the system.

Strictly speaking, the term "entangled" does not mean here quantum entanglement, but only reflects quantum superposition at the one-electron level. Although spin-orbit coupling generally describes the interaction of spin and orbital operators and mixing of corresponding degrees of freedom, its impact depends strongly on the specific state: for the AFO-oe phase it is the main one, and for other phases, it is secondary. Besides, for the FM-eO phase there is the phase change of t_{2g} orbital amplitude going from one sublattice to another: two sublattices differ by this sign only. Obviously, such a mixing can be taken into account within HFA.

For the sake of completeness, we also performed optimization of the crystal structure for uniform and not too high pressure of 10 GPa (at very high P, the system is expected to become metallic and the physical mechanism responsible for magnetism and other physical properties will change). We found that the crystal field increases to 64 meV; the hopping turns out to be 295 meV and thus also grows to $\Delta_{CF} = 0.22t$. On the one hand, this works for stabilization of AFO-eO states shifting Sr$_2$VO$_4$ higher and to the left (J_H/t effectively decreases) in the phase diagram of Fig. 5(b). On the other hand, while in the first approximation atomic-like parameters J_H and λ are not expected to change considerably, it is not *a priori* clear how strongly pressure will affect screening of U.

VII. CONCLUSIONS

In this work we considered interplay between different interactions, which define the ground state properties of the three-orbital model on a square lattice with a single electron per site relevant, e.g., for layered perovskites with t_{2g}^1 electronic configuration. The method used—the generalized Hartree-Fock approximation—is suitable to describe the case of strong electronic correlations at other integer filling as well. However, more elaborated approaches such as dynamical mean field theory [52] should be applied in the metallic regime.

We also consider only the checkerboard order and demonstrate that even this very particular case has a rich phase diagram and the spin-orbit coupling changes it dramatically leading to stabilization of several highly unusual states including those where conventional spin moment vanishes and an exotic order of octupolar magnetic moments appears.

There are five different phases according to present calculations: three conventional states with antiferromagnetic and ferro-orbital, AFM-xy, and ferromagnetic and antiferro-orbital orderings, FM-AFO$_{xz/yz}$ and FM-AFO$_{xy/1}$, stabilized by the Kugel-Khomskii mechanism and two other orbital-entangled states—AFO-eO and FM-eO. The ferromagnetic

FM-eO phase is favored by the intra-atomic Hund's exchange and competition of different exchange interaction is ferromagnetic. Another unconventional state, AFO-eO, is promoted by the spin-orbit coupling. This phase was proposed by Jackeli and Khaliullin [20], while the state suggested by Eremin *et al.* [21] turns out to be higher in energy.

It is worth noting that a plethora of various states in the model under consideration is due to two reasons: (1) competition of different interactions (spin-orbit coupling, intersite and intra-atomic exchanges) and (2) symmetry of the problem, which makes hopping processes strongly orbital dependent and anisotropic.

Our consideration can be readily generalized to treat different transition metal compounds with anomalous physical properties related to the spin-orbit coupling and interplay between spin and orbital degrees of freedom, e.g., Ba_2NaOsO_6 [53–56], Ba_2CeIrO_6 [57], or Ba_2CaOsO_6 [58–61]. The results obtained for Sr_2VO_4 demonstrate that this material lies close to the region of the phase diagram, where four out of five states can be realized. Therefore some external perturbation can be used to change physical properties of Sr_2VO_4 shifting it from one to another phase. While most of experimental results have been obtained in previous decades, physical properties of this material are still intriguing and remain unexplained. Present high-precision neutron diffraction experiments with error bar smaller than $0.6\mu_B$ [17] might be useful to resolve the issue with vanishing magnetic moment. In the meantime, other modern experimental techniques [62–64] can be used to study possible octupolar order in Sr_2VO_4.

Theoretically it would be very interesting to include in consideration not only orbital degrees of freedom and the spin-orbit coupling as was done in the present paper, but also to take into account a long-range exchange interaction and its possible anisotropy, since both have been demonstrated to play an important role for Sr_2VO_4 [22].

ACKNOWLEDGMENTS

APPENDIX A: EFFECTIVE MODEL IN A MULTIORBITAL CASE

In this Appendix we derive the effective kinetic Hamiltonian for arbitrary hopping matrix $t_{ij}^{mm'}$ generalizing the classical derivation of Kugel and Khomskii [2]. We consider the Hamiltonian (1) in the case of one electron per site, treating $\mathcal{H}_0 = \mathcal{H}_{CF} + \mathcal{H}_{so} + \mathcal{H}_{Coulomb}$ as the main Hamiltonian and hopping processes described by $\mathcal{H}_{tr}$ as a

perturbation [65],

$$\mathcal{H}_{eff} = \mathcal{P}\mathcal{H}_0\mathcal{P} - \mathcal{P}\mathcal{H}_{tr}\mathcal{H}_0^{-1}(1-\mathcal{P})\mathcal{H}_{tr}\mathcal{P}, \quad (A1)$$

where $\mathcal{P}$ is projection operator on the subspace with one electron at each lattice site. Obviously $\mathcal{P}\mathcal{H}_{Coulomb}\mathcal{P} = 0$ and we neglect the impact of $\mathcal{H}_{CF}$ [see Eq. (3)] and $\mathcal{H}_{so}$ [see Eq. (4)] on the eigenvalues and eigenfunctions of virtual (excited) states:

$$\mathcal{P}\mathcal{H}_{tr}\mathcal{H}_0^{-1}(1-\mathcal{P})\mathcal{H}_{tr}\mathcal{P} \approx \mathcal{P}\mathcal{H}_{tr}\mathcal{H}_{Coulomb}^{-1}(1-\mathcal{P})\mathcal{H}_{tr}\mathcal{P}.$$

This approximation is justified by that $|\Delta_{CF}|, |\lambda| \ll U - 3J_H$.

Our derivation generalizes the derivation of [66] to the case of an arbitrary number of orbitals N_d (in the main text $N_d = 3$). There have been also other approaches proposed to treat the same problem within the method of irreducible operators [67].

There are two types of two-electron states at one site: *doubles*, characterized by double occupancy of a particular orbital (there are N_d such states), and *pair-orbital* states [$2N_d(N_d - 1) = 4 \times N_d(N_d - 1)/2$; factor 4 originates from the spin degeneracy]. These two sets of states form invariant subspaces of $\mathcal{H}_{Coulomb}$.

One can introduce basis functions for the subspace of doubles in the following way,

$$E_{d\Sigma} = U + (N_d - 1)J_H : A_{d\Sigma}^\dagger = \frac{1}{\sqrt{N_d}}\sum_m c_{m\uparrow}^\dagger c_{m\downarrow}^\dagger, \quad (A2)$$

$$E_d = U - J_H : A_{dk}^\dagger = \sum_m a_m^{(k)} c_{m\uparrow}^\dagger c_{m\downarrow}^\dagger, \quad (A3)$$

where E_α are the energies (eigenvalues of $\mathcal{H}_{Coulomb}$) of the corresponding states, $k = 1, \ldots, N_d - 1$, and the coefficients $a_m^{(k)}$ satisfy the relations $\sum_m a_m^{(k)} = 0$ and $\sum_m a_m^{(k)*}a_m^{(k')} = \delta_{kk'}$. We also use the notation $a_m^{(N_d)} = 1/\sqrt{N_d}$, which corresponds to the wave function $A_{d\Sigma}^\dagger$, so that the matrix $a_m^{(k)}$ appears to be unitary.

For the subspace of pair orbitals, we have

$$A_{a:mm'}^\dagger = \frac{1}{\sqrt{2}}\sum_{\sigma\sigma'}\sigma_{\sigma\sigma'}^o c_{m\sigma}^\dagger c_{m'\sigma'}^\dagger, \quad m < m', \quad (A4)$$

with $o = 0, x, y, z$, and there are once again two subspaces—singlet (S) and triplet (T) ones with the energies

$$E_S = U' + J_H : o = y, \quad (A5)$$

$$E_T = U' - J_H : o = 0, x, z. \quad (A6)$$

As a whole, we have four eigenspaces, for which the projectors onto the corresponding excited states can be readily obtained,

$$\mathcal{P}_{d\Sigma} = A_{d\Sigma}^\dagger A_{d\Sigma}, \quad (A7)$$

$$\tilde{\mathcal{P}}_d = \sum_{k=1}^{N_d-1} A_{dk}^\dagger A_{dk}, \quad (A8)$$

$$\mathcal{P}_S = \sum_{m<m'} A_{y:mm'}^\dagger A_{y:mm'}, \quad (A9)$$

$$\mathcal{P}_T = \sum_{o=0,x,z}\sum_{m<m'} A_{a:mm'}^\dagger A_{a:mm'}. \quad (A10)$$

In order to formulate the effective model in the second-order perturbation theory, we have to take the sum over all

subspaces of excited states (given by $\alpha = d\Sigma, d, S, T$),

$$
\mathcal{H}_{\text{eff}} = \mathcal{H}_{\text{CF}} + \mathcal{H}_{\text{so}} - \sum_{\alpha} E_{\alpha}^{-1}
$$

$$
\times \sum_{ijm_1m_1'm_2m_2'\sigma\sigma'} t_{ij}^{m_1m_2'} t_{ji}^{m_1'm_2} c_{im_1\sigma}^{\dagger} c_{im_2\sigma'} c_{jm_2'\sigma'} \mathcal{P}_{j\alpha} c_{jm_1'\sigma}^{\dagger},
$$

(A11)

where $\mathcal{P}_{j\alpha}$ is projector $\mathcal{P}_{\alpha}$ at site j. The last expression describes processes of the electron transfer from site i, orbital m_2, spin projection σ to site j, orbital m_1', and the same spin. Then, we project this excited state onto different subspaces and move the electron back to the initial site. It is convenient for further consideration, however, to rearrange c operators in Eq. (A11) according to the site index. Here and below we assume that $\mathcal{H}_{\text{eff}}$ acts on the subspace with one electron at each lattice site.

Before proceeding to calculating $c_{m\sigma} \mathcal{P}_{\alpha} c_{m'\sigma'}^{\dagger}$, we present explicit expressions for some of the projectors via c operators. From Eq. (A7), one can obtain

$$
\mathcal{P}_{d\Sigma} = \frac{1}{N_d} \sum_{mm'} c_{m\uparrow}^{\dagger} c_{m\downarrow}^{\dagger} c_{m'\downarrow} c_{m'\uparrow},
$$

(A12)

while Eqs. (A2) and (A7) give

$$
\tilde{\mathcal{P}}_d = \sum_{mm'} \sum_{k=1}^{N_d-1} a_m^{(k)} a_{m'}^{(k)*} c_{m\uparrow}^{\dagger} c_{m\downarrow}^{\dagger} c_{m'\downarrow} c_{m'\uparrow}
$$

$$
= \sum_{mm'} (\delta_{mm'} - 1/N_d) c_{m\uparrow}^{\dagger} c_{m\downarrow}^{\dagger} c_{m'\downarrow} c_{m'\uparrow} = \mathcal{P}_d - \mathcal{P}_{d\Sigma},
$$

(A13)

where

$$
\mathcal{P}_d = \sum_{m} c_{m\uparrow}^{\dagger} c_{m\uparrow} c_{m\downarrow}^{\dagger} c_{m\downarrow}
$$

(A14)

is the projector onto subspace of doubles (d). Correspondingly for the triplet pair-orbital state [see definitions (A9) and (A10)], we have

$$
\mathcal{P}_T = \mathcal{B} + \mathcal{P}_S
$$

(A15)

and

$$
\mathcal{B} = \sum_{m<m',\sigma\sigma'} c_{m\sigma}^{\dagger} c_{m\sigma'} c_{m'\sigma'}^{\dagger} c_{m'\sigma},
$$

(A16)

where the Fierz identity,

$$
\sum_{o=0}^{3} \sigma_{\sigma_1\sigma_1'}^{o} \sigma_{\sigma_2\sigma_2'}^{o} = 2\delta_{\sigma_1\sigma_2'}\delta_{\sigma_2\sigma_1'},
$$

(A17)

was used.

Next, we calculate $c_{m\sigma} \mathcal{P}_{\alpha} c_{m'\sigma'}^{\dagger}$ from Eq. (A11) separately for each subspace (omitting the site index j). Equation (A15) allows us to consider $\mathcal{P}_{\alpha} = d\Sigma, d, S,$ and $\mathcal{B}$ (instead of T).

(i) $\alpha = d\Sigma$. From Eq. (A12), we readily find

$$
c_{m\sigma} \mathcal{P}_{d\Sigma} c_{m'\sigma'}^{\dagger} = \frac{1}{N_d} \sum_{m_1m_1'} [c_{m\sigma}, c_{m_1\uparrow}^{\dagger} c_{m_1\downarrow}^{\dagger}][c_{m_1'\downarrow} c_{m_1'\uparrow}, c_{m'\sigma'}^{\dagger}].
$$

(A18)

Here and below, the terms, which are not bilinear form in the Fermi operators, are omitted since they are eventually

projected out of the considered state. Thus, we obtain

$$
c_{m\sigma} \mathcal{P}_{d\Sigma} c_{m'\sigma'}^{\dagger} = (1/N_d)\gamma_{\sigma}\gamma_{\sigma'} c_{m\bar{\sigma}}^{\dagger} c_{m'\bar{\sigma}'},
$$

(A19)

where $\gamma_{\uparrow} = +1$, $\gamma_{\downarrow} = -1$, and finally one gets the expression entering Eq. (A11) for $d\Sigma$ subspace

$$
\sum_{\sigma\sigma'} c_{im_1\sigma}^{\dagger} c_{im_2\sigma'} c_{jm_2'\sigma'} \mathcal{P}_{jd\Sigma} c_{jm_1'\sigma}^{\dagger}
$$

$$
= (1/N_d) \sum_{\sigma\sigma'} c_{im_1\sigma}^{\dagger} c_{im_2\sigma'} \gamma_{\sigma}\gamma_{\sigma'} c_{jm_2'\bar{\sigma}}^{\dagger} c_{jm_1'\bar{\sigma}'}
$$

$$
= (2/N_d)\big(\mathcal{S}_{im_1m_2}^{(0)} \mathcal{S}_{jm_2'm_1'}^{(0)} - \boldsymbol{\mathcal{S}}_{im_1m_2} \boldsymbol{\mathcal{S}}_{jm_2'm_1'}\big),
$$

(A20)

where $\mathcal{S}_{imm'}^{(o)}$ is defined by Eq. (5). Without the orbital index, all its components coincide with the conventional spin (and number of particles) operators. The conventional charge and spin operators are obtained by taking trace of $\mathcal{S}_{imm'}^{(o)}$ over orbital indices.

(ii) $\alpha = d$. Following the same strategy, one can find using Eq. (A14)

$$
c_{m\sigma} \mathcal{P}_d c_{m'\sigma'}^{\dagger} = \sum_{m_1} [c_{m\sigma}, c_{m_1\uparrow}^{\dagger} c_{m_1\downarrow}^{\dagger}][c_{m_1\downarrow} c_{m_1\uparrow}, c_{m'\sigma'}^{\dagger}]
$$

$$
= \delta_{mm'}\gamma_{\sigma}\gamma_{\sigma'} c_{m\bar{\sigma}}^{\dagger} c_{m\bar{\sigma}'},
$$

(A21)

and finally, the expression entering Eq. (A11) in terms of generalized spin operators transforms to

$$
\sum_{\sigma\sigma'} c_{im_1\sigma}^{\dagger} c_{im_2\sigma'} c_{jm_2'\sigma'} \tilde{\mathcal{P}}_{jd} c_{jm_1'\sigma}^{\dagger}
$$

$$
= \big(\delta_{m_1'm_2'} - 1/N_d\big) \sum_{\sigma\sigma'} \gamma_{\sigma}\gamma_{\sigma'} c_{im_1\sigma}^{\dagger} c_{im_2\sigma'} c_{jm_2'\bar{\sigma}}^{\dagger} c_{jm_1'\bar{\sigma}'}
$$

$$
= 2\big(\delta_{m_1'm_2'} - 1/N_d\big)\big(\mathcal{S}_{im_1m_2}^{(0)} \mathcal{S}_{jm_2'm_1'}^{(0)} - \boldsymbol{\mathcal{S}}_{im_1m_2} \boldsymbol{\mathcal{S}}_{jm_2'm_1'}\big).
$$

(A22)

(iii) $\alpha = \mathcal{B}$.

$$
c_{m\sigma}\mathcal{B}c_{m'\sigma'}^{\dagger} = \sum_{m_1<m_1',\sigma_1\sigma_1'} [c_{m\sigma}, c_{m_1\sigma_1}^{\dagger} c_{m_1'\sigma_1'}^{\dagger}][c_{m_1'\sigma_1} c_{m_1\sigma_1'}, c_{m'\sigma'}^{\dagger}]
$$

$$
= \sum_{m_1<m_1',\sigma_1\sigma_1'} \big(\delta_{mm_1}\delta_{\sigma\sigma_1} c_{m_1'\sigma_1'}^{\dagger} - \delta_{mm_1'}\delta_{\sigma\sigma_1'} c_{m_1\sigma_1}^{\dagger}\big)
$$

$$
\times \big(\delta_{m'm_1}\delta_{\sigma'\sigma_1'} c_{m_1'\sigma_1} - \delta_{m'm_1'}\delta_{\sigma'\sigma_1} c_{m_1\sigma_1'}\big).
$$

(A23)

Using symmetry of this expression with respect to the orbital index exchange $m_1 \leftrightarrow m_1'$ we obtain

$$
c_{m\sigma}\mathcal{B}c_{m'\sigma'}^{\dagger} = \delta_{mm'} \sum_{m_1 \neq m} c_{m_1\sigma'}^{\dagger} c_{m_1\sigma} - \delta_{\sigma\sigma'}(1 - \delta_{mm'})
$$

$$
\times \sum_{\sigma_1} c_{m'\sigma_1}^{\dagger} c_{m\sigma_1}.
$$

(A24)

Finally we obtain

$$
\sum_{\sigma\sigma'} c_{im_1\sigma}^{\dagger} c_{im_2\sigma'} c_{jm_2'\sigma'} \mathcal{B}_j c_{jm_1'\sigma}^{\dagger}
$$

$$
= 2\delta_{m_1'm_2'} \sum_{m \neq m_1'} \big(\mathcal{S}_{i;m_1m_2}^{(0)} \mathcal{S}_{j;mm}^{(0)} + \boldsymbol{\mathcal{S}}_{i;m_1m_2} \boldsymbol{\mathcal{S}}_{j;mm}\big)
$$

$$
- 4\big(1 - \delta_{m_1'm_2'}\big)\mathcal{S}_{i;m_1m_2}^{(0)} \mathcal{S}_{j;m_1'm_2'}^{(0)}.
$$

(A25)

(iv) $\alpha = S$.

$$c_{m\sigma}\mathcal{P}_S c_{m'\sigma'}^\dagger = \sum_{m_1 < m_1'} [c_{m\sigma}, A_{y:m_1 m_1'}^\dagger][A_{y:m_1 m_1'}, c_{m'\sigma'}^\dagger], \quad (A26)$$

and since

$$[A_{y:m_1 m_1'}, c_{m\sigma}^\dagger] = (i/\sqrt{2})[c_{m_1'\downarrow}c_{m_1\uparrow} - c_{m_1'\uparrow}c_{m_1\downarrow}, c_{m\sigma}^\dagger]$$
$$= i(\gamma_\sigma/\sqrt{2})(\delta_{mm_1}c_{m_1'\bar\sigma} + \delta_{mm_1'}c_{m_1\bar\sigma}), \quad (A27)$$

we find using $m_1 \leftrightarrow m_1'$ symmetry that

$$c_{m\sigma}\mathcal{P}_S c_{m'\sigma'}^\dagger = \frac{1}{4}\gamma_\sigma\gamma_{\sigma'} \sum_{m_1 \neq m_1'} (\delta_{mm_1}c_{m_1'\bar\sigma}^\dagger + \delta_{mm_1'}c_{m_1\bar\sigma}^\dagger)$$
$$\times (\delta_{m'm_1}c_{m_1'\bar\sigma'} + \delta_{m'm_1'}c_{m_1\bar\sigma'}). \quad (A28)$$

Finally, the expression entering Eq. (A11) for the subspace S is given by

$$\sum_{\sigma\sigma'} c_{im_1\sigma}^\dagger c_{im_2\sigma'} c_{jm_2'\sigma} \mathcal{P}_{jS} c_{jm_1'\sigma'}^\dagger$$
$$= \delta_{m_1'm_2'} \sum_m (1 - 2\delta_{m_1'm})(\mathcal{S}_{im_1m_2}^{(0)}\mathcal{S}_{jmm}^{(0)} - \boldsymbol{\mathcal{S}}_{im_1m_2}\boldsymbol{\mathcal{S}}_{jmm})$$
$$+ \mathcal{S}_{im_1m_2}^{(0)}\mathcal{S}_{jm_1'm_2'}^{(0)} - \boldsymbol{\mathcal{S}}_{im_1m_2}\boldsymbol{\mathcal{S}}_{jm_1'm_2'}. \quad (A29)$$

Using Eq. (A15), we get analogously for the T subspace

$$\sum_{\sigma\sigma'} c_{im_1\sigma}^\dagger c_{im_2\sigma'} c_{jm_2'\sigma} \mathcal{P}_{jT} c_{jm_1'\sigma'}^\dagger$$
$$= \delta_{m_1'm_2'} \sum_m (3\mathcal{S}_{i;m_1m_2}^{(0)}\mathcal{S}_{j;mm}^{(0)} + \boldsymbol{\mathcal{S}}_{i;m_1m_2}\boldsymbol{\mathcal{S}}_{j;mm})$$
$$- 3\mathcal{S}_{i;m_1m_2}^{(0)}\mathcal{S}_{j;m_1'm_2'}^{(0)} - \boldsymbol{\mathcal{S}}_{i;m_1m_2}\boldsymbol{\mathcal{S}}_{j;m_1'm_2'}. \quad (A30)$$

Combining all the results together and summing over the excited states, we arrive at a final expression for the effective Hamiltonian in terms of the generalized spin operators,

$$\mathcal{H}_{\text{eff}} = \mathcal{H}_{\text{CF}} + \mathcal{H}_{\text{so}} - \sum_{ijm_1m_1'm_2m_2'} t_{ij}^{m_1m_2} t_{ji}^{m_1'm_2'} \left\{ -\frac{2J_d}{[U + (N_d - 1)J_d](U - J_d)}\left(\mathcal{S}_{im_1m_2}^{(0)}\mathcal{S}_{jm_2'm_1'}^{(0)} - \boldsymbol{\mathcal{S}}_{im_1m_2}\boldsymbol{\mathcal{S}}_{jm_2'm_1'}\right) \right.$$

$$+ 2\delta_{m_1'm_2'}\left(\frac{1}{U - J_d} - \frac{1}{U' + J_H}\right)\left(\mathcal{S}_{im_1m_2}^{(0)}\mathcal{S}_{jm_2'm_1'}^{(0)} - \boldsymbol{\mathcal{S}}_{im_1m_2}\boldsymbol{\mathcal{S}}_{jm_2'm_1'}\right) + \delta_{m_1'm_2'}\left(\left(\frac{1}{U' + J_H} + \frac{3}{U' - J_H}\right)\mathcal{S}_{im_1m_2}^{(0)}\sum_m \mathcal{S}_{jmm}^{(0)}\right.$$

$$\left. + \left(\frac{1}{U' - J_H} - \frac{1}{U' + J_H}\right)\boldsymbol{\mathcal{S}}_{im_1m_2}\sum_m \boldsymbol{\mathcal{S}}_{jmm}\right) - \left(\frac{3}{U' - J_H} - \frac{1}{U' + J_H}\right)\mathcal{S}_{im_1m_2}^{(0)}\mathcal{S}_{jm_1'm_2'}^{(0)}$$

$$\left. - \left(\frac{1}{U' - J_H} + \frac{1}{U' + J_H}\right)\boldsymbol{\mathcal{S}}_{im_1m_2}\boldsymbol{\mathcal{S}}_{jm_1'm_2'}\right\}. \quad (A31)$$

For the hopping parameters, which are diagonal in the orbital space $t_{ij}^{mm'} = \delta_{mm'}t_{ij}^m$, using the Kanamori parametrization [25] $U' = U - 2J_H$, $J_d = J_H$ and taking into account that $\sum_m \mathcal{S}_{jmm}^{(0)} = 1/2$, one obtains

$$\mathcal{H}_{\text{eff}} = \mathcal{H}_{\text{CF}} + \mathcal{H}_{\text{so}}$$

$$- \sum_{ijm} t_{ij}^m t_{ji}^m \left[\frac{1}{2}\left(\frac{1}{U - J_H} + \frac{3}{U - 3J_H}\right)\mathcal{S}_{imm}^{(0)}\right.$$

$$\left. + \left(\frac{1}{U - 3J_H} - \frac{1}{U - J_H}\right)\boldsymbol{\mathcal{S}}_{imm}\mathbf{S}_j\right]$$

$$+ \sum_{ijm_1m_2} t_{ij}^{m_1} t_{ji}^{m_2} \left[\frac{2J_d}{[U + (N_d - 1)J_H](U - J_H)}\right.$$

$$\times \left(\mathcal{S}_{im_1m_2}^{(0)}\mathcal{S}_{jm_1m_2}^{(0)} - \boldsymbol{\mathcal{S}}_{im_1m_2}\boldsymbol{\mathcal{S}}_{jm_1m_2}\right)$$

$$+ \left(\frac{3}{U - 3J_H} - \frac{1}{U - J_H}\right)\mathcal{S}_{im_1m_2}^{(0)}\mathcal{S}_{jm_2m_1}^{(0)}$$

$$\left. + \left(\frac{1}{U - 3J_H} + \frac{1}{U - J_H}\right)\boldsymbol{\mathcal{S}}_{im_1m_2}\boldsymbol{\mathcal{S}}_{jm_2m_1}\right], \quad (A32)$$

where $\mathbf{S}_i$ is defined by Eq. (25).

Below we consider in detail an application of Eq. (A32) for the calculation of the difference between energies of the AFM-TM and AFO-eO states (see Fig. 8).

Using the mean-field approximation for the Hamiltonian (A32) is equivalent to the assumption that Φ has a two-sublattice form,

$$\Phi = \prod_{i_1 \in A}\prod_{i_2 \in B} a_{i_1}^\dagger b_{i_2}^\dagger |0\rangle, \quad (A33)$$

where $|0\rangle$ is vacuum, and site one-electron state a corresponds to sublattice A and b to sublattice B. Then $E_{\text{kin}} = \langle\Phi|\mathcal{H}_{\text{kin}}|\Phi\rangle$. Under this approximation we have to replace charge-spin operators in Eq. (A36) by their averages. So we have to calculate $\langle\mathcal{S}_{imm'}^{(0)}\rangle$ and $\langle\boldsymbol{\mathcal{S}}_{imm'}\rangle$ to calculate the energy of the state Φ.

Omitting site index i and writing generally for $d = a, b$

$$d^\dagger = \sum_{m\sigma} u_{m\sigma}^d c_{m\sigma}^\dagger, \quad (A34)$$

with $u_{m\sigma}$ being arbitrary normalized coefficients, we get

$$\langle\mathcal{S}_{mm'}^{(o)}\rangle_d = \frac{1}{2}\sum_{\sigma\sigma'} \sigma_{\sigma\sigma'}^{(o)}(u_{m\sigma}^d)^* u_{m'\sigma'}^d. \quad (A35)$$
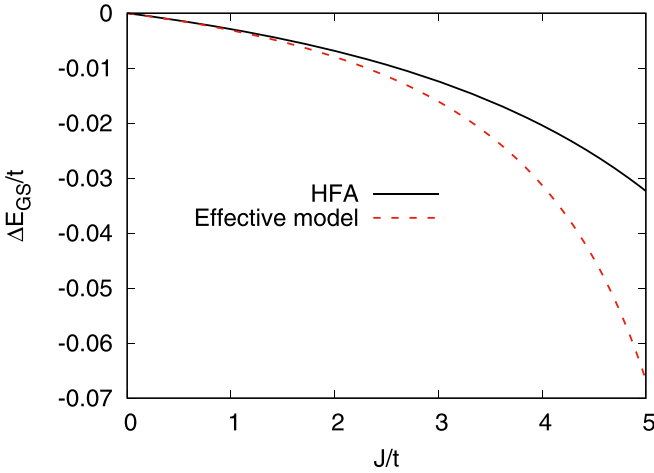
FIG. 8. Total energy difference between AFM-TM and AFO-eO states for $U = 20t$, $\Delta_{CF} = 0$, $\lambda = 0$ as obtained by the direct calculation using Hartree-Fock methods (black solid line) and effective model for kinetic exchange within the mean-field approximation developed in Appendix A (red dashed line); see Eq. (26).

Since the xy orbital is not occupied we simplify the expression (A32) for energy taking into account in the sum over m_1, m_2 only diagonal terms ($m_1 = m_2$),

$$
\begin{aligned}
E_{\mathrm{kin}}(\Phi) = \sum_{ij,m_1 \neq xy} |t_{ij}^{m_1}|^2 & \left[-\frac{\langle s_{im_1}^{(0)} \rangle}{2} \left(\frac{1}{U - J_{\mathrm{H}}} + \frac{3}{U - 3J_{\mathrm{H}}} \right) \right. \\
& - \left(\frac{1}{U - 3J_{\mathrm{H}}} - \frac{1}{U - J_{\mathrm{H}}} \right) \langle s_{im_1} \rangle \langle \mathbf{S}_j \rangle \\
& + \frac{2J_{\mathrm{H}}}{(U + 2J_{\mathrm{H}})(U - J_{\mathrm{H}})} \\
& \times \left(\langle s_{im_1}^{(0)} \rangle \langle s_{jm_1}^{(0)} \rangle - \langle s_{im_1} \rangle \langle s_{jm_1} \rangle \right) \\
& + \left(\frac{3}{U - 3J_{\mathrm{H}}} - \frac{1}{U - J_{\mathrm{H}}} \right) \langle s_{im_1}^{(0)} \rangle \langle s_{jm_1}^{(0)} \rangle \\
& \left. + \left(\frac{1}{U - 3J_{\mathrm{H}}} + \frac{1}{U - J_{\mathrm{H}}} \right) \langle s_{im_1} \rangle \langle s_{jm_1} \rangle \right], \quad \text{(A36)}
\end{aligned}
$$

where the spin $s_{im}^{(o)} \equiv \mathcal{S}_{imm}^{(o)}$ operator of an orbital m at a site i is introduced.

Now we consider separately $E_{\mathrm{kin}}(\Phi)$ for TAFM and oe-AFM states.

(i) AFM-TM order. We assume that

$$a^\dagger = -\frac{1}{\sqrt{2}}(i c_{xz\uparrow}^\dagger + c_{yz\uparrow}^\dagger), \quad \text{(A37)}$$

$$b^\dagger = -\frac{1}{\sqrt{2}}(i c_{xz\downarrow}^\dagger - c_{yz\downarrow}^\dagger), \quad \text{(A38)}$$

so $u_{m\sigma}^{a,b} = -i\delta_{m,xz}/\sqrt{2} \mp \delta_{m,xy}/\sqrt{2}$.

We get from Eq. (A35)

$$\langle s_m^{(o)} \rangle_{\mathrm{A}} = \frac{1}{4}\sigma_{\uparrow\uparrow}^{(o)}(1 - \delta_{m,xy}), \quad \text{(A39)}$$

$$\langle s_m^{(o)} \rangle_{\mathrm{B}} = \frac{1}{4}\sigma_{\downarrow\downarrow}^{(o)}(1 - \delta_{m,xy}). \quad \text{(A40)}$$

(ii) AFO-eO order.

$$a^\dagger = -\frac{1}{2}(i c_{xz\uparrow}^\dagger + c_{yz\uparrow}^\dagger + i c_{xz\downarrow}^\dagger - c_{yz\downarrow}^\dagger), \quad \text{(A41)}$$

$$b^\dagger = -\frac{1}{2}(i c_{xz\uparrow}^\dagger + c_{yz\uparrow}^\dagger - i c_{xz\downarrow}^\dagger + c_{yz\downarrow}^\dagger), \quad \text{(A42)}$$

so $u_{m\sigma}^a = -i\delta_{m,xz}/2 - \gamma_\sigma \delta_{m,yz}/2$, $u_{m\sigma}^b = -i\gamma_\sigma\delta_{m,xz}/2 - \delta_{m,yz}/2$, $\gamma_\sigma = +1(-1)$ for $\sigma = \uparrow (\downarrow)$. We get analogously

$$\langle s_m^{(o)} \rangle_{\mathrm{A,B}} = \frac{1}{4}\delta_{a,0}(\delta_{m,xz} + \delta_{m,yz}) \pm \frac{1}{4}\delta_{a,x}(\delta_{m,xz} - \delta_{m,yz}). \quad \text{(A43)}$$

Note that for neighboring sites i and j, both orders $\langle s_{im}^{(0)} \rangle \langle s_{jm}^{(0)} \rangle = 1/16$, $\langle \mathbf{s}_{im} \rangle \langle \mathbf{s}_{jm} \rangle = -1/16$. Therefore all terms in Eq. (A36) coincide besides underlined term. In the case AFM-TM order we get $\langle \mathbf{S}_i \rangle = (-1)^i \mathbf{e}_z/2$ with unit vector directed along z axis $\mathbf{e}_z$; therefore $\langle \mathbf{s}_{im_1} \rangle \langle \mathbf{S}_j \rangle = -1/8$. This term has a different nature than another terms in Eq. (A36) since here *total* spin exhibits *ferromagnetic* exchange interaction with spin of neighbor orbitals (indexed by m_1). In the case of AFO-eO order $\langle \mathbf{S}_j \rangle = 0$. We find that ferromagnetic exchange interaction increases the energy of TAFM order making it less favorable than AFO-eO order due to a delicate effect of ferromagnetic exchange interaction.

APPENDIX B: INTERORBITAL COULOMB INTERACTION HAMILTONIAN WITHIN HFA

In this Appendix we present a HFA treatment of the local Coulomb Hamiltonian $\mathcal{H}_{\mathrm{Coulomb}}$ (8), Appendix B 1, and use this for the derivation of the total HFA Hamiltonian, see Eq. (15), Appendix B 2.

1. Coulomb interaction Hamiltonian treatment

We write the Coulomb interaction Hamiltonian omitting for brevity site index

$$
\begin{aligned}
\mathcal{H}_{\mathrm{Coulomb}} = & \frac{U}{2} \sum_{m\sigma} c_{m\sigma}^\dagger c_{m\bar\sigma}^\dagger c_{m\bar\sigma} c_{m\sigma} + \frac{J_d}{2} \sum_{m\neq m';\sigma} c_{m\sigma}^\dagger c_{m\bar\sigma}^\dagger c_{m'\bar\sigma} c_{m'\sigma} \\
& + \frac{U'}{2} \sum_{m\neq m'\sigma\sigma'} c_{m\sigma}^\dagger c_{m'\sigma'}^\dagger c_{m'\sigma'} c_{m\sigma} \\
& + \frac{J_{\mathrm{H}}}{2} \sum_{m\neq m';\sigma\sigma'} c_{m\sigma}^\dagger c_{m'\sigma'}^\dagger c_{m\sigma'} c_{m'\sigma}. \quad \text{(B1)}
\end{aligned}
$$

This sum is rewritten as

$$\mathcal{H}_{\mathrm{Coulomb}} = \sum_{\beta = U, J_d, U', J_{\mathrm{H}}} \mathcal{H}_{\mathrm{int}}[W^{(\beta)}], \quad \text{(B2)}$$

where

$$\mathcal{H}_{\mathrm{int}}[W] = \frac{1}{2} \sum_{mm'm_1 m_1' \sigma\sigma'} W_{\sigma\sigma'}(mm'; m_1 m_1') c_{m\sigma}^\dagger c_{m'\sigma'}^\dagger c_{m_1'\sigma'} c_{m_1\sigma} \quad \text{(B3)}$$

and

$$W_{\sigma\sigma'}^{(U)} = U \cdot (1 - \delta_{\sigma\sigma'}) \delta_{mm'} \delta_{mm_1} \delta_{mm_1'}, \quad \text{(B4)}$$

$$W_{\sigma\sigma'}^{(U')} = U'(1 - \delta_{mm'}) \delta_{mm_1} \delta_{m'm_1'}, \quad \text{(B5)}$$

$$W_{\sigma\sigma'}^{(J_{\mathrm{H}})} = J_{\mathrm{H}}(1 - \delta_{mm'}) \delta_{mm_1'} \delta_{m'm_1}, \quad \text{(B6)}$$

$$W_{\sigma\sigma'}^{(J_d)} = J_d(1 - \delta_{\sigma\sigma'}) \cdot (1 - \delta_{mm_1}) \delta_{mm'} \delta_{m_1 m_1'}, \quad \text{(B7)}$$

where arguments of $W^{(\beta)}(mm'; m_1 m_1')$ are omitted for brevity.

The HFA treatment of all terms is performed in an equal way ($\mathcal{H}_{\text{int}}[W^{(\beta)}] \to \mathcal{H}_{\text{int}}^{\text{HFA}}[W^{(\beta)}]$) using the Wick theorem:

$$
\begin{aligned}
\mathcal{H}_{\text{int}}^{\text{HFA}}[W^{(\beta)}] = &\sum_{mm'm_1m_1'\sigma\sigma'} W_{\sigma\sigma'}^{(\beta)}(mm'; m_1 m_1') \\
&\times \big(c_{m\sigma}^{\dagger} c_{m_1\sigma} \langle c_{m'\sigma'}^{\dagger} c_{m_1'\sigma'} \rangle \\
&- c_{m\sigma}^{\dagger} c_{m_1'\sigma'} \langle c_{m'\sigma'}^{\dagger} c_{m_1\sigma} \rangle \big) - E_{\text{DC}}^{(\beta)},
\end{aligned} \tag{B8}
$$

where $E_{\text{DC}}^{(\beta)}$ is introduced to avoid double counting and equals half of the statistical average of the first two terms.

For the case $\beta = U, J_{\text{d}}$ the spin projection dependence reads $W_{\sigma\sigma'}^{(\beta)}(mm'; m_1 m_1') \propto (1 - \delta_{\sigma\sigma'})$ and we rewrite σ sums in Eq. (B8) through generalized density and spin operators, see Eq. (5),

$$
\begin{aligned}
\mathcal{H}_{\text{int}}^{\text{HFA}}[W^{(\beta)}] = &\sum_{mm'm_1m_1'} W_{\uparrow\downarrow}^{(\beta)}(mm'; m_1 m_1') \\
&\times \big(2\mathcal{S}_{mm_1}^{(0)} \mathfrak{n}_{m'm_1'} - 2\mathcal{S}_{mm_1}^{z} \mathfrak{m}_{m'm_1'}^{z} \\
&- \mathcal{S}_{mm_1'}^{+} \mathfrak{m}_{m'm_1}^{-} - \mathcal{S}_{mm_1'}^{-} \mathfrak{m}_{m'm_1}^{+} \big) - E_{\text{DC}}^{(\beta)}. \tag{B9}
\end{aligned}
$$

Here for $\beta = U$ we get from Eq. (B4)

$$
\mathcal{H}_{\text{int}}^{\text{HFA}}[W^{(U)}] = 2U \sum_{m} \big(\mathcal{S}_{mm}^{(0)} \mathfrak{n}_{mm} - \mathcal{S}_{mm}^{z} \mathfrak{m}_{mm}^{z} \big) - E_{\text{DC}}^{(U)}, \tag{B10}
$$

and for $\beta = J_{\text{d}}$ we get from Eq. (B7)

$$
\mathcal{H}_{\text{int}}^{\text{HFA}}[W^{(J_{\text{d}})}] = 2J_{\text{d}} \sum_{m \neq m_1} \big(\mathcal{S}_{mm_1}^{(0)} \mathfrak{n}_{mm_1} - \mathcal{S}_{mm_1}^{z} \mathfrak{m}_{mm_1}^{z} \big) - E_{\text{DC}}^{(J_{\text{d}})}. \tag{B11}
$$

For the case $\beta = U', J_{\text{H}}$ $W^{(\beta)}$ is spin independent, so we rewrite Eq. (B8)

$$
\begin{aligned}
\mathcal{H}_{\text{int}}^{\text{HFA}}[W^{(\beta)}] = &2 \sum_{mm'm_1m_1'} W_{\uparrow\downarrow}^{(\beta)}(mm'; m_1 m_1') \\
&\times \big(2\mathcal{S}_{mm_1}^{(0)} \mathfrak{n}_{m'm_1'} - \mathcal{S}_{mm_1'}^{(0)} \mathfrak{n}_{m'm_1} - \mathcal{S}_{mm_1'} \mathfrak{m}_{m'm_1} \big) \\
&- E_{\text{DC}}^{(\beta)}. \tag{B12}
\end{aligned}
$$

Here for $\beta = U'$ we get from Eq. (B5)

$$
\begin{aligned}
\mathcal{H}_{\text{int}}^{\text{HFA}}[W^{(U')}] = &2U' \sum_{m \neq m'} \big(2\mathcal{S}_{mm}^{(0)} \mathfrak{n}_{m'm'} \\
&- \mathcal{S}_{mm'}^{(0)} \mathfrak{n}_{m'm} - \mathcal{S}_{mm'} \mathfrak{m}_{m'm} \big) - E_{\text{DC}}^{(U')}, \tag{B13}
\end{aligned}
$$

and for $\beta = J_{\text{H}}$ we get from Eq. (B6)

$$
\begin{aligned}
\mathcal{H}_{\text{int}}^{\text{HFA}}[W^{(J_{\text{H}})}] = &2J_{\text{H}} \sum_{m \neq m'} \big(2\mathcal{S}_{mm'}^{(0)} \mathfrak{n}_{m'm} - \mathcal{S}_{mm}^{(0)} \mathfrak{n}_{m'm'} \\
&- \mathcal{S}_{mm} \mathfrak{m}_{m'm'} \big) - E_{\text{DC}}^{(J_{\text{H}})}. \tag{B14}
\end{aligned}
$$

We write down the final mean-field version of the Coulomb Hamiltonian as

$$
\mathcal{H}_{\text{Coulomb}}^{\text{HFA}} = 2 \sum_{mm'} \big(\mathcal{F}_{mm'}^{(0)} \mathcal{S}_{mm'}^{(0)} - \mathbf{\mathcal{F}}_{mm'} \mathbf{\mathcal{S}}_{mm'} \big) - E_{\text{DC}}, \tag{B15}
$$

where the contributions from four above-considered terms are collected together,

$$
\begin{aligned}
\mathcal{F}_{mm'}^{(0)} = &\delta_{mm'}[(2U' - J_{\text{H}})K + \delta U \mathfrak{n}_{mm}] \\
&+ (2J_{\text{H}} - U')\mathfrak{n}_{m'm} + J_{\text{d}}\mathfrak{n}_{mm'}, \tag{B16}
\end{aligned}
$$

$$
\mathbf{\mathcal{F}}_{mm'} = \delta_{mm'}[J_{\text{H}}\mathbf{M} + \delta U \mathfrak{m}_{mm}] + U'\mathfrak{m}_{m'm} + J_{\text{d}}\mathfrak{m}_{mm'}, \tag{B17}
$$

$$
E_{\text{DC}} = \sum_{mm'} \big(\mathcal{F}_{mm'}^{(0)} \mathfrak{n}_{mm'} - \mathbf{\mathcal{F}}_{mm'} \mathfrak{m}_{mm'} \big), \tag{B18}
$$

where $\delta U = U - U' - J_{\text{H}} - J_{\text{d}}$, where

$$
K = \sum_{m} \mathfrak{n}_{mm}, \tag{B19}
$$

$$
\mathbf{M} = \sum_{m} \mathfrak{m}_{mm}. \tag{B20}
$$

Within the Kanamori approximation $\delta U = 0$ and we employ this in the main text.

2. Derivation of HFA Hamiltonian

Below we present details of the HFA approximation for the Hamiltonian (1), using the results of Appendix B 1 of this Appendix, restoring the site index i.

We apply the transformation to the Bloch wave functions in Eq. (9),

$$
c_{im\sigma} = N^{-1/2} \sum_{\mathbf{k}} \exp(-i\mathbf{k}\mathbf{R}_i) c_{\mathbf{k}m\sigma}, \tag{B21}
$$

and the Fourier transform of $C_{m\sigma;m'\sigma'}^{i}$ turns out to be

$$
C_{m\sigma;m'\sigma'}(\mathbf{q}) = \frac{1}{N} \sum_{\mathbf{k}} \langle c_{\mathbf{k}m\sigma}^{\dagger} c_{\mathbf{k}+\mathbf{q},m'\sigma'} \rangle. \tag{B22}
$$

The result of application of HFA to the Hamiltonian (8) is

$$
\begin{aligned}
\mathcal{H}_{\text{Coulomb}}^{\text{MF}} = &\sum_{\mathbf{k}\mathbf{k}'} \sum_{\sigma\sigma'} \sum_{mm'} \big[\mathcal{F}_{mm'}^{(0)}(\mathbf{k} - \mathbf{k}')\delta_{\sigma\sigma'} \\
&- \mathbf{\mathcal{F}}_{mm'}(\mathbf{k} - \mathbf{k}')\mathbf{\sigma}_{\sigma\sigma'} \big] c_{\mathbf{k}m\sigma}^{\dagger} c_{\mathbf{k}'m'\sigma'}, \tag{B23}
\end{aligned}
$$

where mean fields $\mathcal{F}_{mm'}^{(0)}(\mathbf{k} - \mathbf{k}')$ and $\mathbf{\mathcal{F}}_{mm'}(\mathbf{k} - \mathbf{k}')$ are Fourier transforms of mean fields given by Eqs. (16) and (17).

The treatment of the Hamiltonian (15) is presented below. We introduce the magnetic Brillouin zone ($|k_x| + |k_y| < \pi$), so that for any $\mathbf{k}_1$ from the Brillouin zone we have a presentation $\mathbf{k}_1 = \mathbf{k} + \alpha\mathbf{Q}$, where $\alpha = 0, 1$. We rewrite Eq. (15) through the summation over the magnetic Brillouin zone (denoted by a prime)

$$
\mathcal{H}_{\text{MF}} = \sideset{}{'}\sum_{\mathbf{k}\alpha\alpha';mm'} \sum_{\sigma\sigma'} H_{m\sigma\alpha;m'\sigma'\alpha'}^{\text{MF}}(\mathbf{k}) c_{\mathbf{k}+\alpha\mathbf{Q},m\sigma}^{\dagger} c_{\mathbf{k}+\alpha'\mathbf{Q},m'\sigma'}, \tag{B24}
$$

where the $\mathbf{k}$-dependent $3 \times 2 \times 2$ matrix

$$
\begin{aligned}
H^{\mathrm{MF}}_{m\alpha\sigma;m'\alpha'\sigma'}(\mathbf{k}) = & \Big\{ [\varepsilon_{mm'}(\mathbf{k}+\alpha\mathbf{Q}) + \Delta_{\mathrm{CF}}\delta_{m,xy}]\delta_{mm'}\delta_{\sigma\sigma'} \\
& + \mathcal{F}^{(0)\mathrm{u}}_{mm'}\delta_{\sigma\sigma'} - \boldsymbol{\mathcal{F}}^{\mathrm{u}}_{mm'}\boldsymbol{\sigma}_{\sigma\sigma'} - (\lambda/2)\mathbf{l}_{mm'}\boldsymbol{\sigma}_{\sigma\sigma'} \Big\} \\
& \times \delta_{\alpha\alpha'} + \big[\mathcal{F}^{(0)\mathrm{s}}_{mm'}\delta_{\sigma\sigma'} - \boldsymbol{\mathcal{F}}^{\mathrm{s}}_{mm'}\boldsymbol{\sigma}_{\sigma\sigma'} \big]\delta_{\alpha\tilde{\alpha}'}
\end{aligned}
$$

$$\text{(B25)}$$

is introduced. Here $\varepsilon_{mm'}(\mathbf{k})$ sets up the band spectrum, the explicit expression for which is given in the end of Sec. II.

The Hamiltonian matrix (B25) is diagonalized by the transformation (cf. [68])

$$
c_{\mathbf{k}+\alpha\mathbf{Q},m\sigma} = \sum_\nu a_{m\alpha\sigma;\nu}(\mathbf{k})d_{\mathbf{k}\nu}.
\tag{B26}
$$

In terms of new Fermi operators $d_{\mathbf{k}\nu}$, $d^\dagger_{\mathbf{k}\nu}$ the Hamiltonian has the form

$$
\mathcal{H}_{\mathrm{MF}} = \sum_{\mathbf{k}\nu}{}' E_\nu(\mathbf{k})d^\dagger_{\mathbf{k}\nu}d_{\mathbf{k}\nu}.
\tag{B27}
$$

Then the correlator (B22) can be expressed through the spectrum $E_\nu(\mathbf{k})$ and coefficients $a_{m\alpha\sigma;\nu}(\mathbf{k})$:

$$
\langle c^\dagger_{\mathbf{k}+\alpha\mathbf{Q},m\sigma}c_{\mathbf{k}'+\alpha'\mathbf{Q},m'\sigma'}\rangle = \delta_{\mathbf{kk}'}\sum_\nu a^*_{m\alpha\sigma;\nu}(\mathbf{k})a_{m'\alpha'\sigma';\nu}(\mathbf{k})f(E_\nu(\mathbf{k})).
$$

$$\text{(B28)}$$

Applying Eq. (B18) we obtain

$$
\begin{aligned}
E_{\mathrm{DC}}/N = \sum_{\mathbf{q}=0,\mathbf{Q}} \Bigg\{ & (2U' - J_{\mathrm{H}})K^2(\mathbf{q}) - J_{\mathrm{H}}\mathbf{M}^2(\mathbf{q}) \\
& + \delta U \sum_m \big[\mathfrak{n}^2_{mm}(\mathbf{q}) - \mathfrak{m}^2_{mm}(\mathbf{q}) \big] \\
& + J_{\mathrm{d}} \sum_{mm'} \big[\mathfrak{n}^2_{mm'}(\mathbf{q}) - \mathfrak{m}^2_{mm'}(\mathbf{q}) \big] \\
& - (U' - 2J_{\mathrm{H}}) \sum_{mm'} \mathfrak{n}_{mm'}(\mathbf{q})\mathfrak{n}_{m'm}(\mathbf{q}) \\
& - U' \sum_{mm'} \mathfrak{m}_{mm'}(\mathbf{q}) \cdot \mathfrak{m}_{m'm}(\mathbf{q}) \Bigg\}.
\end{aligned}
$$

$$\text{(B29)}$$

[1] D. Khomskii and K. Kugel, Solid State Commun. **13**, 763 (1973).

[2] K. I. Kugel and D. I. Khomskii, Sov. Phys. Usp. **25**, 231 (1982).

[3] K. Nelson, Z. Mao, Y. Maeno, and Y. Liu, Science **306**, 1151 (2004).

[4] V. Anisimov, I. Nekrasov, D. Kondakov, T. Rice, and M. Sigrist, Eur. Phys. J. B **25**, 191 (2002).

[5] B. J. Kim, H. Jin, S. J. Moon, J.-Y. Kim, B.-G. Park, C. S. Leem, J. Yu, T. W. Noh, C. Kim, S.-J. Oh, J.-H. Park, V. Durairaj, G. Cao, and E. Rotenberg, Phys. Rev. Lett. **101**, 076402 (2008).

[6] Q. Li, X. Yuan, L. Xing, and M. Xu, Sci. Rep. **6**, 27712 (2016).

[7] J. Matsuno, Y. Okimoto, Z. Fang, X. Z. Yu, Y. Matsui, N. Nagaosa, M. Kawasaki, and Y. Tokura, Phys. Rev. Lett. **93**, 167202 (2004).

[8] S. K. Pandey, Phys. Rev. B **81**, 035114 (2010).

[9] H. Wu, Phys. Rev. B **86**, 075120 (2012).

[10] X. L. Wang and E. Takayama-Muromachi, Phys. Rev. B **72**, 064401 (2005).

[11] K. W. Lee and W. E. Pickett, Phys. Rev. B **73**, 174428 (2006).

[12] S. Bhardwaj and S. K. Pandey, arXiv:2401.05149.

[13] T. Ishikawa, T. Toriyama, T. Konishi, H. Sakurai, and Y. Ohta, J. Phys. Soc. Jpn. **86**, 033701 (2017).

[14] B. Pandey, Y. Zhang, N. Kaushal, R. Soni, L.-F. Lin, W.-J. Hu, G. Alvarez, and E. Dagotto, Phys. Rev. B **103**, 045115 (2021).

[15] M.-C. Lee, C. Occhialini, J. Li, Z. Zhu, N. S. Sirica, L. Mix, S. Kim, D. A. Yarotski, R. Comin, and R. P. Prasankumar, Commun. Phys. **5**, 335 (2022).

[16] T. Yamauchi, T. Shimazu, D. Nishio-Hamane, and H. Sakurai, Phys. Rev. Lett. **123**, 156601 (2019).

[17] M. Cyrot, B. Lambert-Andron, J. L. Soubeyroux, M. J. Rey, P. H. Dehauht, J. Beille, and J. L. Tholence, J. Solid State Chem. **85**, 321 (1990).

[18] J. Sugiyama, H. Nozaki, I. Umegaki, W. Higemoto, E. J. Ansaldo, J. H. Brewer, H. Sakurai, T.-H. Kao, H.-D. Yang, and M. Månsson, Phys. Rev. B **89**, 020402(R) (2014).

[19] Y. Imai, I. Solovyev, and M. Imada, Phys. Rev. Lett. **95**, 176405 (2005).

[20] G. Jackeli and G. Khaliullin, Phys. Rev. Lett. **103**, 067205 (2009).

[21] M. V. Eremin, J. Deisenhofer, R. M. Eremina, J. Teyssier, D. van der Marel, and A. Loidl, Phys. Rev. B **84**, 212407 (2011).

[22] B. Kim, S. Khmelevskyi, P. Mohn, and C. Franchini, Phys. Rev. B **96**, 180405(R) (2017).

[23] A. Abragam and B. Bleaney, *Electron Paramagnetic Resonance of Transition Ions* (Oxford University Press, New York, 1970).

[24] S. Streltsov and D. Khomskii, Phys. Usp. **60**, 1121 (2017).

[25] J. Kanamori, Prog. Theor. Phys. **30**, 275 (1963).

[26] V. Y. Irkhin and A. Entelis, J. Phys.: Condens. Matter **1**, 4111 (1989).

[27] A. Pankratova, P. Igoshev, and V. Y. Irkhin, J. Phys.: Condens. Matter **33**, 375802 (2021).

[28] G. Kotliar and A. E. Ruckenstein, Phys. Rev. Lett. **57**, 1362 (1986).

[29] P. A. Igoshev, M. A. Timirgazin, V. F. Gilmutdinov, A. K. Arzhnikov, and V. Y. Irkhin, J. Phys.: Condens. Matter **27**, 446002 (2015).

[30] P. Igoshev, M. Timirgazin, A. Arzhnikov, and V. Y. Irkhin, J. Magn. Magn. Mater. **459**, 311 (2018).

[31] M. Katsnelson and V. Y. Irkhin, J. Phys. C **17**, 4291 (1984).

[32] P. A. Igoshev and V. Y. Irkhin, Phys. Rev. B **104**, 045109 (2021).

[33] J. B. Goodenough, *Magnetism and the Chemical Bond* (Wiley, New York, 1963).

[34] D. I. Khomskii, *Transition Metal Compounds* (Cambridge University Press, Cambridge, 2014).

[35] D. Khomskii and S. Streltsov, Chem. Rev. **121**, 2992 (2021).

[36] S. V. Streltsov, A. S. Mylnikova, A. O. Shorikov, Z. V. Pchelkina, D. I. Khomskii, and V. I. Anisimov, Phys. Rev. B **71**, 245114 (2005).

[37] J.-H. Lee, T. Shishidou, and A. J. Freeman, Phys. Rev. B **66**, 233102 (2002).

[38] P. A. Igoshev, S. V. Streltsov, and K. I. Kugel, J. Magn. Magn. Mater. **587**, 171315 (2023).

[39] S. V. Streltsov and D. I. Khomskii, Phys. Rev. X **10**, 031043 (2020).

[40] S. V. Streltsov, F. V. Temnikov, K. I. Kugel, and D. I. Khomskii, Phys. Rev. B **105**, 205142 (2022).

[41] P. Santini, S. Carretta, G. Amoretti, R. Caciuffo, N. Magnani, and G. H. Lander, Rev. Mod. Phys. **81**, 807 (2009).

[42] J. P. Perdew, K. Burke, and M. Ernzerhof, Phys. Rev. Lett. **77**, 3865 (1996).

[43] G. Kresse and J. Furthmüller, Phys. Rev. B **54**, 11169 (1996).

[44] P. E. Blöchl, Phys. Rev. B **50**, 17953 (1994).

[45] P. E. Blöchl, O. Jepsen, and O. K. Andersen, Phys. Rev. B **49**, 16223 (1994).

[46] M. Schüler, O. E. Peil, G. J. Kraberger, R. Pordzik, M. Marsman, G. Kresse, T. O. Wehling, and M. Aichhorn, J. Phys.: Condens. Matter **30**, 475901 (2018).

[47] S. Mohapatra, D. K. Singh, R. Ray, S. Ghosh, and A. Singh, J. Phys.: Condens. Matter **35**, 045801 (2023).

[48] R. Arita, J. Kuneš, A. V. Kozhevnikov, A. G. Eguiluz, and M. Imada, Phys. Rev. Lett. **108**, 086403 (2012).

[49] B. Kim and C. Franchini (private communication).

[50] R. Arita, A. Yamasaki, K. Held, J. Matsuno, and K. Kuroki, J. Phys.: Condens. Matter **19**, 365204 (2007).

[51] G. C. Moore, M. K. Horton, E. Linscott, A. M. Ganose, M. Siron, D. D. O'Regan, and K. A. Persson, Phys. Rev. Mater. **8**, 014409 (2024).

[52] N. Samani, G. Zhang, and E. Pavarini, Phys. Rev. Lett. **132**, 236505 (2024).

[53] A. S. Erickson, S. Misra, G. J. Miller, R. R. Gupta, Z. Schlesinger, W. A. Harrison, J. M. Kim, and I. R. Fisher, Phys. Rev. Lett. **99**, 016404 (2007).

[54] D. F. Mosca, L. V. Pourovskii, B. H. Kim, P. Liu, S. Sanna, F. Boscherini, S. Khmelevskyi, and C. Franchini, Phys. Rev. B **103**, 104401 (2021).

[55] L. Lu, M. Song, W. Liu, A. P. Reyes, P. Kuhns, H. O. Lee, I. R. Fisher, and V. F. Mitrović, Nat. Commun. **8**, 14407 (2017).

[56] D. F. Mosca, H. Schnait, L. Celiberti, M. Aichhorn, and C. Franchini, Comput. Mater. Sci. **233**, 112764 (2024).

[57] A. Revelli, C. C. Loo, D. Kiese, P. Becker, T. Fröhlich, T. Lorenz, M. M. Sala, G. Monaco, F. L. Buessen, J. Attig *et al.*, Phys. Rev. B **100**, 085139 (2019).

[58] S. Voleti, D. D. Maharaj, B. D. Gaulin, G. Luke, and A. Paramekanti, Phys. Rev. B **101**, 155118 (2020).

[59] L. V. Pourovskii, D. F. Mosca, and C. Franchini, Phys. Rev. Lett. **127**, 237201 (2021).

[60] C. M. Thompson, J. P. Carlo, R. Flacau, T. Aharen, I. Leahy, J. Pollichemi, T. J. S. Munsie, T. Medina, G. M. Luke, J. Munevar *et al.*, J. Phys.: Condens. Matter **26**, 306003 (2014).

[61] G. Khaliullin, D. Churchill, P. P. Stavropoulos, and H.-Y. Kee, Phys. Rev. Res. **3**, 033163 (2021).

[62] R. Sibille, N. Gauthier, E. Lhotel, V. Porée, V. Pomjakushin, R. A. Ewings, T. G. Perring, J. Ollivier, A. Wildes, C. Ritter *et al.*, Nat. Phys. **16**, 546 (2020).

[63] N. Sasabe, M. Kimata, and T. Nakamura, Phys. Rev. Lett. **126**, 157402 (2021).

[64] S. W. Lovesey and D. D. Khalyavin, Phys. Rev. B **103**, 235160 (2021).

[65] S. V. Tyablikov, *Methods in the Quantum Theory of Magnetism* (Plenum Press, New York, 1967).

[66] C. Castellani, C. R. Natoli, and J. Ranninger, Phys. Rev. B **18**, 4945 (1978).

[67] V. Yu. Irkhin and Y. P. Irkhin, J. Exp. Theor. Phys. **77**, 858 (1993).

[68] P. A. Igoshev, M. A. Timirgazin, A. A. Katanin, A. K. Arzhnikov, and V. Y. Irkhin, Phys. Rev. B **81**, 094407 (2010).